



**HAL**  
open science

# Thermo-rheological reduced order models for non-Newtonian fluid flows with power-law viscosity via the modal identification method

Manuel Girault, Qiao Lin, Nadine Allanic, Pierre Mousseau

## ► To cite this version:

Manuel Girault, Qiao Lin, Nadine Allanic, Pierre Mousseau. Thermo-rheological reduced order models for non-Newtonian fluid flows with power-law viscosity via the modal identification method. *International Journal of Heat and Mass Transfer*, 2023, 203, pp.123692. 10.1016/j.ijheatmasstransfer.2022.123692 . hal-04281468

**HAL Id: hal-04281468**

**<https://hal.science/hal-04281468>**

Submitted on 13 Nov 2023

**HAL** is a multi-disciplinary open access archive for the deposit and dissemination of scientific research documents, whether they are published or not. The documents may come from teaching and research institutions in France or abroad, or from public or private research centers.

L'archive ouverte pluridisciplinaire **HAL**, est destinée au dépôt et à la diffusion de documents scientifiques de niveau recherche, publiés ou non, émanant des établissements d'enseignement et de recherche français ou étrangers, des laboratoires publics ou privés.

# Thermo-rheological Reduced Order Models for non-Newtonian fluid flows with power-law viscosity via the Modal Identification Method

Manuel GIRAULT<sup>1\*</sup>, Qiao LIN<sup>2</sup>, Nadine ALLANIC<sup>2</sup>, Pierre MOUSSEAU<sup>2</sup>

<sup>1</sup> Institut PPRIME UPR CNRS 3346 - CNRS ◊ ISAE-ENSMA ◊ Université de Poitiers  
ENSMA, Téléport 2, 1 avenue Clément ADER, BP 40109  
F-86961 Futuroscope Chasseneuil CEDEX, France

<sup>2</sup> GEPEA Nantes Université, Oniris, CNRS, GEPEA, UMR 6144 F-44000 Nantes, France

\* corresponding author: [manuel.girault@ensma.fr](mailto:manuel.girault@ensma.fr)

## Abstract

In the framework of melted polymer flows characterization, this study deals with the formulation, construction and validation of thermo-rheological Reduced Order Models (ROMs) for incompressible flows of pseudoplastic fluids. The dynamic viscosity is described by a shear rate power law defined by consistency index  $K$  and pseudoplastic index  $n$ . The flow dynamics are assumed to be quasi-static whereas the thermal state is unsteady. Viscous dissipation acts as a heat source term in the energy equation. ROMs are built through the Modal Identification Method (MIM). First, their general form is derived from governing local conservation equations and the viscosity power-law, with an original approach to handle the issues related to the pseudoplastic index  $n$ . Then ROMs are identified using Particle Swarm Optimization and Ordinary Least Squares, from simulations coming from a reference Full Order Model (FOM). The approach is applied to a polymer flow in an annular duct, corresponding to an experimental lab apparatus. ROMs allow computing temperature at chosen locations of interest whatever the applied inputs, here parameters  $K$ ,  $n$  and inlet flowrate as well as a time-varying volumetric heat source power in the central axis. Compared to the reference Finite Elements FOM, computing time is considerably reduced with limited loss of accuracy.

**Keywords:** generalized Newtonian fluid; pseudoplastic fluid; elastomer; low order model; model identification; data assimilation

## Nomenclature

$a^v$	ROM state vector for $v \in \{T, p, g, \eta\}$	$\bar{g}_a$	gravity acceleration vector (m.s <sup>-2</sup> )
$a^v$	ROM state vector for velocity $\bar{v}$	$H$	output matrix of ROM
$b^g, b^\eta$	intermediate state vectors in ROM for viscosity	$\mathcal{J}_{ident}^{(m)}$	quadratic functional to be minimized for identifying ROM of order $m$
$C_p$	specific heat (J.kg <sup>-1</sup> .K <sup>-1</sup> )	$K$	consistency index (Pa.s <sup><math>n</math></sup> )
$\bar{D}$	strain rate tensor (s <sup>-1</sup> )	$L$	length of annular part (m)
$e$	thickness of outer wall (m)	$m$	order of ROM
$g$	scalar function defined as $\dot{\gamma}^2$ (s <sup>-2</sup> )	$n$	pseudoplastic index (-)

$\bar{n}$  local outward normal unit vector  
 $N_{obs}$  number of observable temperatures  
 $N_{param}$  number of ROM parameters  
 $N_s$  number of sets (triplets  $K, n, Q_{in}$ )  
 $N_t$  number of instants  
 $N_\theta$  size of parameter vector  $\theta$   
 $p$  pressure (Pa)  
 $\bar{q}$  heat flux vector ( $W.m^{-2}$ )  
 $Q_{in}$  inlet flowrate ( $cc.s^{-1}$ )  
 $r$  radial coordinate (m)  
 $R$  outer radius of annular duct (m)  
 $S$  volumetric heat source ( $W.m^{-3}$ )  
 $t$  time (s)  
 $T$  temperature (K)  
 $T_{init}$  initial uniform temperature (K)  
 $T_{obs}$  observable temperature (K)  
 $\bar{v}$  velocity vector ( $m.s^{-1}$ )  
 $\bar{x}$  position vector (m)  
 $z$  axial coordinate (m)

#### Abbreviations

FOM Full order model  
 MIM Modal Identification Method  
 ROM Reduced order model

#### Greek symbols

$\dot{\gamma}$  shear rate ( $s^{-1}$ )  
 $\dot{\bar{\gamma}}$  generalized shear rate ( $s^{-1}$ )  
 $\Gamma$  boundary  
 $\delta T$  temperature deviation w.r.t.  $T_{init}$  (K)  
 $\delta T_{obs}$  observable temperature deviation w.r.t.  $T_{init}$  (K)  
 $\varepsilon_v$  viscous dissipation ( $W.m^{-3}$ )

$\eta$  dynamic viscosity (Pa.s)  
 $\theta$  vector of ROM constitutive parameters (except components of  $H$ )  
 $\kappa$  ratio of inner radius to outer radius  
 $\lambda$  thermal conductivity ( $W.m^{-1}.K^{-1}$ )  
 $\Pi(a, a')$  vector of nonlinearities involving two state vectors  $a$  and  $a'$   
 $\Pi^*(a)$  vector of nonlinearities involving a single state vector  $a$   
 $\rho$  density ( $kg.m^{-3}$ )  
 $\sigma^{(m)}$  mean quadratic error between outputs of FOM and ROM of order  $m$  (K)  
 $\bar{\tau}$  viscous stress tensor (Pa)  
 $\varphi$  heat flux density ( $W.m^{-2}$ )  
 $\phi^v$  space function for  $v \in \{T, p, g, \eta\}$   
 $\bar{\phi}^v$  space vector function for velocity  $\bar{v}$   
 $\chi_s$  distribution function for heat source  
 $\Omega$  domain

#### Subscripts

d Dirichlet boundary condition  
 f or  $f$  fluid  
*ident* relative to ROM identification  
 in or *in* inlet  
 n Neumann boundary condition  
 out outlet  
 s or  $s$  solid  
*set* relative to a specific set ( $K, n, Q_{in}$ )  
 sf solid/fluid interface  
*valid* relative to ROM validation

#### Superscripts

*id* relative to ROM identification  
*val* relative to ROM validation

# 1 Introduction

Complex flow structure modeling is widely studied for industrial or research purpose. For example, in the field of plastic processing where the melt temperature depends on the viscous dissipation and the thermal regulation system, it is important to not only measure flow variables (pressure, temperature, etc.) directly in molds (which have usually complex geometries) [1] but also be able to simulate the system in such circumstances [2]. Thanks to their accuracy, Finite element models can be used for process analysis and optimization [3], mold design [4] and production quality improvement [5], however their use in industry is limited by their complexity. Moreover, due to their time-consuming drawbacks, these models are rarely used with process control strategies [6] [7] or for in-line viscosity identification/monitoring tools [8]. For applications such as in-line thermo-rheological characterization in transient state via inverse method, an efficient (or even analytically derivable) model is needed [9].

A ROM is a model involving a small number of degrees of freedom (dof) and able to reproduce the behavior of an actual system or a reference model of this system (model with a large number of dof sometimes called full order model (FOM) or detailed model), whatever the (possibly time-varying) boundary conditions and source terms and/or for a range of values of some parameters. A ROM may be obtained by reduction of a FOM or identified from data coming either from simulations of a FOM or from measurements on the actual system (experimental set-up or industrial plant for instance). One of the most known and used methods for building ROMs is the POD-Galerkin approach, where the ROM equations are obtained via a Galerkin projection of local governing equations on space functions coming from Proper Orthogonal Decomposition (POD) performed over data covering space and time. In order to compute these space functions, it is required for data to cover the entire spatial domain or at least a part of it for which the ROM is built (a 2D plane in a 3D problem for instance). As an example, Wang et al. used POD-Galerkin in [10] for building a ROM for two-dimensional Rayleigh-Bénard convection flow of a viscoelastic fluid. The Proper Generalized Decomposition (PGD) appears to provide a discrete solution in physical space, time and possibly parameters space rather than a continuous ROM. In [11], Chinesta et al. gathered applications of PGD to some rheology-related problems. In particular, PGD was used in [12] by Aghighi et al. to compute the transient solution of a two-dimensional Rayleigh-Bénard flow model for both Newtonian fluids and non-Newtonian power-law fluids. In [13], Hernandez-Martinez et al. studied a laminar flow of a power-law viscoelastic fluid in a circular duct, subject to periodic variations of the pressure gradient. A reduced model was obtained by approximating the nonlinearities associated to shear stress with the first-harmonic Fourier basis.

The present paper is a follow-up of our previous work on model reduction for generalized Newtonian fluids [14], where references to other existing model reduction methods (many of

them having not been yet applied to non-Newtonian fluid flows) can be found. In the present work, the Modal Identification Method (MIM) [14] [15] [16] [17] [18] [19] is used to build ROMs. As in many model reduction methods, each variable field (e.g. temperature, velocity, etc.) is written as a linear combination of space functions with coefficients depending on time and/or on some parameters. As in POD-Galerkin, MIM requires the knowledge of the local governing equations. In the MIM approach, the ROM equations may also be written down using a Galerkin projection [14] [18] [19] but only the form of these equations is important. Whereas in POD-Galerkin, the components of the ROM constitutive elements are computed using their literal expressions depending on the space functions obtained from POD, in the MIM these components are identified through a parameter estimation problem corresponding to the minimization of a quadratic functional based on the difference between some reference output data characterizing the system behavior, on the one hand, and the ROM outputs corresponding to the same inputs, on the other hand [15]. Thus, using data fields over the entire spatial domain is not required to apply MIM: it is possible to build ROMs for a restricted set of observables located at chosen locations. MIM does not aim at obtaining ‘spatial modes’ such as POD modes that can be used to conduct physical analysis. MIM mainly aims at building ROMs acting as a kind of ‘transfer function’ linking inputs to outputs, with the objective to use these ROMs instead of large FOMs, for specific tasks. In addition, MIM does not require to perform a POD on the data. However, the parameter estimation problem requires to use optimization algorithms (Particle Swarm Optimization [20] and Ordinary Least Squares).

MIM was applied on several heat transfer problems, especially for the resolution of inverse and state-feedback control problems. For instance, in [16], ROMs identified from experimental data on thermal system with both radiative and convective boundary conditions were used for solving a transient inverse heat conduction problem for simultaneous estimation of time-varying powers of two internal heat sources from surface temperature measurements. In [17], ROMs built in-situ allowed successful real-time temperature regulation within 0.01°C of an ultra-high precision metrology device by model predictive control. In [18], MIM was used to build ROMs for an incompressible 2D laminar mixed convection flow of a Newtonian fluid around a heated circular cylinder. In [19] was shown the ability of the MIM to be used in the context of conduction and radiation inside semi-transparent media for buildings ROMs having as inputs two parameters (thermal conductivity and effective absorption coefficient) and an applied time-varying applied heat flux density.

In our previous work on model reduction for polymer flows [14], thermo-rheological ROMs were developed for an incompressible flow of a pseudoplastic fluid in a circular duct, taking into account transport, conduction and heat dissipation due to viscous effects in high shear zones. The ROMs, whose output was the temperature profile in the channel outlet section, were explicitly parametrized by two parameters: the consistency index  $K$  and the pseudoplastic index  $n$  defining the power-law model of dynamic viscosity. The analytical velocity profile used in the energy equation for both the transport and viscous dissipation terms induced the presence of terms  $r^{\frac{n+1}{n}}$  where  $r$  is the radial coordinate. As a consequence,

the radial direction was in fact “irreducible” due to its intrinsic link to  $n$ . Therefore, the identification of radial space functions was required to build the ROMs in [14].

In comparison to the work in [14], the present work aims at several improvements:

- The geometry is not limited to a circular cylinder and can be more complex;
- The knowledge of the analytical velocity field is not required;
- The issues related to the pseudoplastic index  $n$  are handled in an original way, allowing a full reduction in all space directions: no space functions need to be computed for the ROMs construction;
- Transient heat transfer is considered;
- In addition to parameters  $K$  and  $n$ , ROMs also have as inputs the inlet flowrate and possible time-varying boundary conditions and/or heat source terms;

Local governing equations and general boundary conditions are presented in section 2, before a brief overview of the MIM in section 3. The development of the ROM equations and their numerical resolution are described in section 4, with details given in Appendix, including an original approach to handle the issues involved by the pseudoplastic index. The method for building the ROMs is presented in section 5, with additional information about the optimization algorithms given in Appendix. In section 6, the approach is applied to a polymer flow in an annular duct, corresponding to an experimental lab apparatus.

## 2 Local governing equations and boundary conditions

### 2.1 Local governing equations

Let us first consider the general case of an incompressible 3D unsteady flow of a viscous fluid in a domain that may also contain some solid parts. Flow equations will nevertheless be used since equations in solid parts are in fact a particular case of these equations. Let us call  $\Omega$  the global domain and  $\Gamma$  its boundary. The problem may be either 2D or 3D. Notations used for a vector  $u$  and a tensor  $A$  are respectively  $\bar{u}$  and  $\bar{A}$ . However, vectors in the ROM equations will be written without symbol for easier reading.

The flow is described by local conservation equations for mass, momentum and energy. The heat flux is assumed to follow Fourier’s law ( $\bar{q} = -\lambda \overline{\text{grad}T}$ ) and the viscous dissipation  $\varepsilon_v$  due to shear is taken into account in the energy equation.

$$\text{div}(\bar{v}) = 0 \tag{1}$$

$$\rho \left( \frac{\partial \bar{v}}{\partial t} + \overline{\text{div}(\bar{v} \otimes \bar{v})} \right) = -\overline{\text{grad}p} + \overline{\text{div}(\bar{\tau})} + \rho \overline{g_a} \quad (2)$$

$$\rho C_p \left( \frac{\partial T}{\partial t} + \text{div}(T\bar{v}) \right) = \text{div}(\lambda \overline{\text{grad}T}) + \chi_S S(t) + \varepsilon_v \quad (3)$$

In order to simplify notations,  $\bar{v} = \bar{v}(\bar{x}, t)$ ,  $p = p(\bar{x}, t)$  and  $T = T(\bar{x}, t)$  denote respectively the velocity vector, pressure and temperature at local position  $M$  defined by vector  $\bar{x}$  and at time  $t$ .

Density  $\rho$ , specific heat capacity  $C_p$  and thermal conductivity  $\lambda$  are assumed to be independent of temperature and *a priori* non-uniform for both fluid and solid in the domain  $\Omega$ . However, in order to lighten notations, they will be noted  $\rho, C_p, \lambda$  rather than  $\rho(\bar{x}), C_p(\bar{x}), \lambda(\bar{x})$  in the following.  $\overline{g_a}$  is the gravity acceleration vector.

Although the transport terms  $\overline{\text{div}(\bar{v} \otimes \bar{v})}$  in eq.(2) and  $\rho C_p \text{div}(T\bar{v})$  in eq.(3) can be written in a simplified manner using eq.(1) i.e. the incompressibility of the flow, they are kept in these forms to ease further mathematical operations.

In eq.(3),  $\varepsilon_v$  is the viscous dissipation term, characteristic of highly viscous flows such as polymer ones where shear induces heat dissipation.

Eq.(3) is used for the fluid domain and also for the solid parts for which heat diffusion is the lone transfer mode ( $\bar{v} = \bar{0}$  and  $\varepsilon_v = 0$ ).

The term  $\chi_S S(t)$  in eq.(3) corresponds to a heat source uniformly distributed on a sub-domain  $\Omega_{\text{source}}$  of  $\Omega$ , typically inside a solid part. The source delivers a time-varying volumetric power  $S(t)$  and  $\chi_S = \chi_S(\bar{x})$  is defined as  $\chi_S = 1$  if  $M \in \Omega_{\text{source}}$  and  $\chi_S = 0$  if  $M \notin \Omega_{\text{source}}$ .

### 2.1.1 Assumption: neglected inertial and buoyancy terms

Due to the small values of Reynolds number in polymer flows, the inertial terms and the buoyancy term  $\rho \overline{g_a}$  in Eq.(2) are assumed to be negligible compared to the viscous terms [21]. Eq.(2) hence writes:

$$\overline{\text{grad}p} = \overline{\text{div}(\bar{\tau})} \quad (4)$$

### 2.1.2 Viscous stress tensor $\bar{\tau}$

For an incompressible flow (eq.(1)) of a generalized Newtonian fluid, the viscous stress tensor  $\bar{\tau}$  (in Pa) is written as:

$$\bar{\tau} = 2\eta\bar{D} \quad (5)$$

Where  $\bar{D}$  is the strain-rate tensor defined as:

$$\bar{D} = \frac{1}{2} \left( \overline{\text{grad}(\bar{v})} + \left( \overline{\text{grad}(\bar{v})} \right)^T \right) \quad (6)$$

And  $\eta$  is the dynamic viscosity of the fluid. Whereas  $\eta$  is constant in the case of Newtonian fluids, it depends on the strain-rate tensor  $\bar{D}$  in the case of generalized Newtonian fluids.

In a simple shear flows,  $\eta(\bar{D})$  reduces to  $\eta(\dot{\gamma})$  where  $\dot{\gamma}$  is the shear rate. For tridimensional complex flows,  $\eta(\bar{D})$  is written as  $\eta(\dot{\gamma})$ , i.e. a function of the generalized shear rate  $\dot{\gamma}$  defined as follows (see [21] for instance):

$$\dot{\gamma} = 2\sqrt{J_2(\bar{D})} \quad (7)$$

Where  $J_2(\bar{D})$  is a second invariant of the strain-rate tensor  $\bar{D}$ :

$$J_2(\bar{D}) = \frac{1}{2} \text{trace}(\bar{D} \cdot \bar{D}) = \frac{1}{2} \bar{D} : \bar{D} \quad (8)$$

Where “ : ” is the symbol for the double-dot product of two tensors.

Taking into account equations (7) and (8), one gets:

$$\dot{\gamma} = \sqrt{2\text{trace}(\bar{D} \cdot \bar{D})} = \sqrt{2\bar{D} : \bar{D}} \quad (9)$$

It should be noted that the usual notation  $\dot{\gamma}$  for the generalized shear rate is used although  $\dot{\gamma}$  is a scalar function.

### 2.1.3 Viscous dissipation term $\varepsilon_v$

In eq.(3), the viscous dissipation term  $\varepsilon_v$  is defined as:

$$\varepsilon_v = \bar{\tau} : \bar{D} \quad (10)$$

Introducing eq.(5) in eq.(10) and using eq.(9) yields:

$$\varepsilon_v = 2\eta\bar{D} : \bar{D} = \eta\dot{\gamma}^2 \quad (11)$$

Using eq.(6),  $\varepsilon_v$  given by eq.(11) can be expressed as a function of velocity:

$$\varepsilon_v = \frac{\eta}{2} \left( \overline{\text{grad}(\bar{v})} + \left( \overline{\text{grad}(\bar{v})} \right)^T \right) : \left( \overline{\text{grad}(\bar{v})} + \left( \overline{\text{grad}(\bar{v})} \right)^T \right) \quad (12)$$

The viscous dissipation term  $\varepsilon_v$  is thus cubic in variables  $\eta$  and  $\bar{v}$ .

In order to limit the number of constitutive parameters to be identified for building the reduced order models, it is preferable to use quadratic functions rather than cubic ones. For that reason, an intermediate function is now introduced.

### 2.1.4 Introduction of intermediate scalar function $g$

Let us define the scalar function  $g(\bar{x})$ , quadratic in  $\dot{\bar{\gamma}}$  and thus quadratic in  $\bar{v}$  :

$$g = \dot{\bar{\gamma}}^2 \stackrel{\text{eq.(9)}}{\equiv} 2\bar{D}:\bar{D} \stackrel{\text{eq.(6)}}{\equiv} \frac{1}{2} \left( \overline{\text{grad}(\bar{v})} + \left( \overline{\text{grad}(\bar{v})} \right)^T \right) : \left( \overline{\text{grad}(\bar{v})} + \left( \overline{\text{grad}(\bar{v})} \right)^T \right) \quad (13)$$

Injecting eq.(13) in eq.(11),  $\varepsilon_v$  is written as a quadratic function of  $\eta$  and  $g$ :

$$\varepsilon_v = \eta g \quad (14)$$

This allows us to work with two quadratic equations (13) and (14) instead of cubic eq.(12).

### 2.1.5 Viscosity model

During a polymer process (e.g. extrusion, injection), the shear rate range is mostly located in the pseudo-plastic zone of viscosity curves [21]. In this zone where the viscosity depends highly on the shear rate, the viscosity variation due to the temperature as well as the Newtonian zone of viscosity curves can be neglected [22] [23]. This assumption will be further discussed in section 6 (application). The polymer melt is assumed to be pseudoplastic following the power law model [24] [25]:

$$\eta = K \dot{\bar{\gamma}}^{n-1} \quad (15)$$

where  $K$  is the *consistency index* and  $n$  is the *power index*. For pseudoplastics fluids, which exhibit shear-thinning,  $n < 1$  is called *pseudoplastic index*.

More complex models such as “Cross fluid” [26] and “Carreau fluid” [27] also contain power-law type expressions. As the main difficulty for handling viscosity in ROMs is due to the presence of a power of a variable (see section A.1.4 of the Appendix), we chose to use the simple power-law model (15), whose interest was demonstrated in [28], in order to demonstrate the feasibility to build thermo-rheological reduced order models for generalized Newtonian fluids, even for more complex viscosity models using power-law type expressions.

Taking into account eq.(13), the dynamic viscosity power-law model (15) is written as:

$$\eta = K g^{\frac{n-1}{2}} \quad (16)$$

### 2.1.6 Final form of local conservation equations

Using eq.(5) and eq.(6), the momentum conservation equation (4) is written as:

$$\overline{\text{grad}p} = \overline{\text{div}} \left( \eta \left( \overline{\text{grad}(\bar{v})} + \left( \overline{\text{grad}(\bar{v})} \right)^T \right) \right) \quad (17)$$

Using eq.(14), the energy conservation equation (3) writes:

$$\frac{\partial T}{\partial t} + \text{div}(T\bar{v}) = \frac{1}{\rho C_p} \text{div}(\lambda \overline{\text{grad}T}) + \frac{\chi_s}{\rho C_p} S(t) + \frac{\eta g}{\rho C_p} \quad (18)$$

Equation (18) is quadratic in the variables  $T, \bar{v}, \eta, g$  because of terms  $\text{div}(T\bar{v})$  and  $\frac{\eta g}{\rho C_p}$ .

In the following, conservation equations (1), (17) and (18) as well as equations (13) and (16) will be used.

### 2.1.7 Poisson equation for pressure

Although the Poisson equation for pressure, obtained by taking the divergence of momentum conservation equation (17), is not used to solve the flow and heat transfer problems, it will be used in the development of the ROM equations. It is given by equation (19) below:

$$\text{div}(\overline{\text{grad}p}) = \text{div}\left(\overline{\text{div}}\left(\eta\left(\overline{\text{grad}}(\bar{v}) + \left(\overline{\text{grad}}(\bar{v})\right)^T\right)\right)\right) \quad (19)$$

## 2.2 Initial and boundary conditions

Figure 1 shows an arbitrary domain  $\Omega$  composed of a solid medium (domain  $\Omega_s$ ) crossed by a fluid flow (domain  $\Omega_f$ ).  $\Gamma_{sf}$  gathers all internal boundaries between solid and fluid domains. The boundary of global domain  $\Omega = \Omega_s \cup \Omega_f$  is  $\Gamma = \Gamma_{in} \cup \Gamma_{out} \cup \Gamma_n \cup \Gamma_d$ . The boundary of fluid domain  $\Omega_f$  is  $\Gamma_f = \Gamma_{in} \cup \Gamma_{out} \cup \Gamma_{sf}$ . The sub-domain  $\Omega_{source}$  is a part of  $\Omega$  in which an internal volumetric heat source is uniformly distributed, as stated in section 2.1. The local outward unit vector normal to the boundary is noted  $\bar{n}$ .

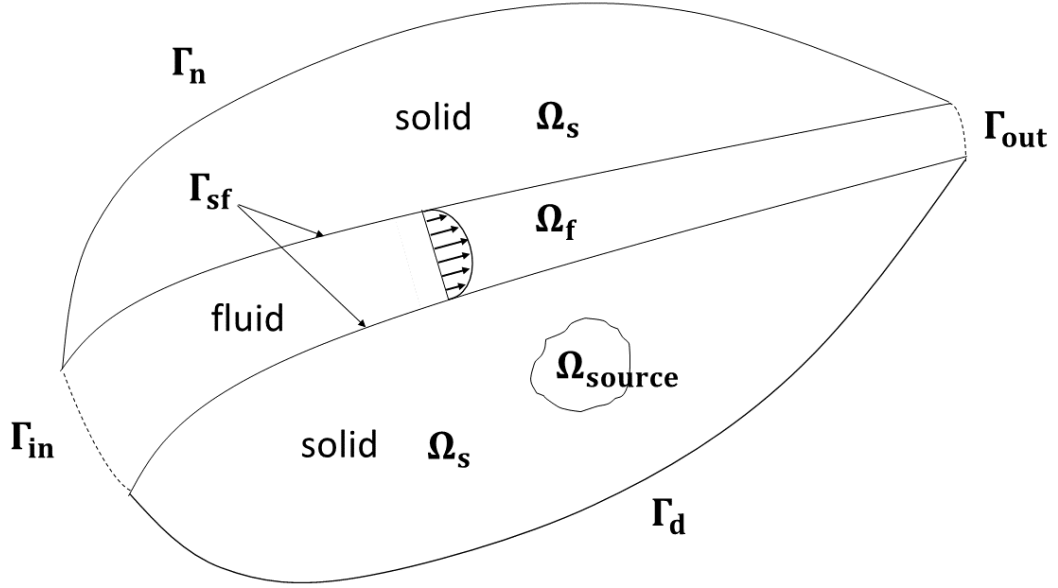


Figure 1. domain  $\Omega = \Omega_s \cup \Omega_f$  with boundary  $\Gamma = \Gamma_{in} \cup \Gamma_{out} \cup \Gamma_n \cup \Gamma_d$ . Fluid domain  $\Omega_f$  with boundary  $\Gamma_f = \Gamma_{in} \cup \Gamma_{out} \cup \Gamma_{sf}$ .

At  $t = 0$ , the fluid is motionless and the temperature field may be non-uniform.

For  $t > 0$ , the fluid flow is assumed to be quasi-static whereas the thermal state is unsteady. It means that at  $t = 0^+$ , fields of velocity, function  $g$  and dynamic viscosity reach instantaneously their respective steady states  $\bar{v}(\bar{x})$ ,  $g(\bar{x})$ ,  $\eta(\bar{x})$ , whereas the transient temperature field  $T(\bar{x}, t)$  starts to change.

Functions  $F_{v_{in}}(\bar{x})$ ,  $F_{T_{in}}(\bar{x})$ ,  $F_{\varphi}(\bar{x})$ ,  $F_{T_w}(\bar{x})$  are used to define spatial distributions for respective following boundary conditions (20), (21), (24), (25). Except for condition (20) for which a constant multiplying parameter  $Q_{in}$  is used, these spatial distributions are multiplied by a time-varying function, respectively  $T_{in}(t)$ ,  $\varphi(t)$ ,  $T_w(t)$  for boundary conditions (21), (24), (25).

Hydrodynamic and thermal boundary conditions on the different parts of boundary  $\Gamma$  are as follows:

- On the fluid flow inlet boundary  $\Gamma_{in}$ :

$$\bar{v} = -F_{v_{in}}(\bar{x})Q_{in}\bar{n} \quad \forall \bar{x} \in \Gamma_{in} \quad (20)$$

Where  $Q_{in} = -\int_{\Gamma_{in}} \bar{v} \cdot \bar{n} d\Gamma$  is the inlet flowrate (thus  $\int_{\Gamma_{in}} F_{v_{in}}(\bar{x}) d\Gamma = 1$ ).

$$T = F_{T_{in}}(\bar{x})T_{in}(t) \quad \forall \bar{x} \in \Gamma_{in}, \forall t \in [0; t_{final}] \quad (21)$$

- On the fluid flow outlet boundary  $\Gamma_{out}$ :

$$\overline{\text{grad}(\bar{v})} \cdot \bar{n} = \bar{0} \quad \forall \bar{x} \in \Gamma_{out} \quad (22)$$

$$\lambda \overline{\text{grad}T} \cdot \bar{n} = 0 \quad \forall \bar{x} \in \Gamma_{\text{out}}, \forall t \in [0; t_{\text{final}}] \quad (23)$$

- On the  $\Gamma_n$  part of the solid boundary (“n” for Neumann):

$$\lambda \overline{\text{grad}T} \cdot \bar{n} = F_\varphi(\bar{x})\varphi(t) \quad \forall \bar{x} \in \Gamma_n, \forall t \in [0; t_{\text{final}}] \quad (24)$$

- On the  $\Gamma_d$  part of the solid boundary (“d” for Dirichlet):

$$T = F_{T_w}(\bar{x})T_w(t) \quad \forall \bar{x} \in \Gamma_d, \forall t \in [0; t_{\text{final}}] \quad (25)$$

In addition, on interface  $\Gamma_{\text{sf}}$  between solid and fluid domains, a no-slip boundary condition is set for velocity:

$$\bar{v} = \bar{0} \quad \forall \bar{x} \in \Gamma_{\text{sf}} \quad (26)$$

Note : the thermal boundary condition on  $\Gamma_{\text{sf}}$  (usually continuity of temperature and heat flux density) is not going to be used in the following because energy equation (18) will be considered on the global domain  $\Omega = \Omega_s \cup \Omega_f$  with boundary  $\Gamma = \Gamma_{\text{in}} \cup \Gamma_{\text{out}} \cup \Gamma_n \cup \Gamma_d$ .

### 3 Modal Identification Method: overview

We aim at building a ROM able to compute temperature values at some specific locations inside the domain and/or on its boundaries as a function of boundary conditions, heat sources, values of parameters  $K$  and  $n$  defining the dynamic viscosity and inlet flowrate  $Q_{\text{in}}$ .

The approach used in the present paper is the Modal Identification Method (MIM) [14] [15] [16] [17] [18] [19]. The MIM consists of three main steps:

- 1) Defining the structure of the ROM equations able to adequately describe the involved physics (see section 4);
- 2) Generating some input-output data representative of the system. Those data may come from in-situ measurements or, as in the present work, from numerical simulations (see section 5.1 for a brief presentation and section 6.2 for the practical application);
- 3) Identifying the fixed constitutive parameters of the ROM equations through the minimization of a functional based on the quadratic residuals between the previously generated output data of the system, on the one hand, and the outputs of the ROM, on the other hand, for the same input data (see section 5.2 for a description of technical aspects and section 6.2 for results on the presented application).

The MIM therefore aims to adjust the ROM constitutive parameters using optimization techniques, in order for the ROM to mimic the data characterizing the input-output responses of the system.

Once identified, the ROMs can be tested using input parameters different than those used for their construction (see section 6.3 for results on the presented application).

## 4 Reduced Order Model formulation

### 4.1 Approximation of fields of variables

The first step consists in approximating fields of variables as sums of space functions weighted by coefficients. These coefficients are time functions for the temperature whereas they are constant for the other variables associated with the steady flow. The coefficients  $a_i^T(t)$  for temperature,  $a_i^v$  for velocity, etc., also depend on parameters  $K, n$  and  $Q_{in}$ , however this will be omitted in notations for easier reading.

The temperature field is thus written as:

$$T(\bar{x}, t) \approx \sum_{i=1}^{m_T} \phi_i^T(\bar{x}) a_i^T(t) \quad (27)$$

Where the  $\phi_i^{(T)}(\bar{x}), i \in \{1, \dots, m_T\}$ , are a truncation of an orthonormal basis of the Hilbert space formed by the space  $\mathcal{L}_2(\Omega)$  of square integrable functions on  $\Omega$  equipped with the inner product  $\langle \cdot, \cdot \rangle_{\rho C_p}$  weighted by the thermal heat capacity  $\rho(\bar{x})C_p(\bar{x})$ :

$$\langle f_1, f_2 \rangle_{\rho C_p} = \int_{\Omega} \rho C_p f_1 f_2 d\Omega \quad (28)$$

Orthonormality of functions  $\phi_i^{(T)}(\bar{x}), i \in \{1, \dots, m_T\}$  for the weighted inner product (28) corresponds to the following property:

$$\langle \phi_i^T, \phi_j^T \rangle_{\rho C_p} = \int_{\Omega} \rho C_p \phi_i^T \phi_j^T d\Omega = \delta_{ij} \quad \forall (i, j) \in \{1, \dots, m_T\}^2 \quad (29)$$

The velocity field is written as:

$$\bar{v}(\bar{x}) \approx \sum_{i=1}^{m_v} \bar{\phi}_i^v(\bar{x}) a_i^v \quad (30)$$

Where the  $\bar{\phi}_i^v(\bar{x}), i \in \{1, \dots, m_v\}$ , are a truncation of a basis of the Hilbert space formed by the space  $[\mathcal{L}_2(\Omega_f)]^d$  of square integrable vector functions on  $\Omega_f$  ( $d$  being the problem dimension) equipped with the inner product  $\langle \bar{\cdot}, \bar{\cdot} \rangle_{\Omega_f}$ :

$$\langle \bar{f}_1, \bar{f}_2 \rangle_{\Omega_f} = \int_{\Omega_f} \bar{f}_1 \cdot \bar{f}_2 d\Omega \quad (31)$$

Introducing equation (30) into mass conservation equation (1), one gets :

$$0 = \text{div}(\bar{v}) = \text{div} \left( \sum_{i=1}^{m_v} \bar{\phi}_i^v(\bar{x}) a_i^v \right) = \sum_{i=1}^{m_v} \left( \text{div}(\bar{\phi}_i^v(\bar{x})) \right) a_i^v$$

As this equation must be verified whatever the values of coefficients  $a_i^v$ , that will depend on inlet flowrate  $Q_{in}$  and on rheological parameters  $K$  and  $n$ , the  $\bar{\phi}_i^v(\bar{x})$  verify:

$$\text{div}(\bar{\phi}_i^v(\bar{x})) = 0, \quad \forall \bar{x} \in \Omega_f, \quad \forall i \in \{1, \dots, m_v\} \quad (32)$$

Fields of pressure, viscosity and function  $g$  are respectively written as:

$$p(\bar{x}) \approx \sum_{i=1}^{m_p} \phi_i^p(\bar{x}) a_i^p \quad (33)$$

$$g(\bar{x}) \approx \sum_{i=1}^{m_g} \phi_i^g(\bar{x}) a_i^g \quad (34)$$

$$\eta(\bar{x}) \approx \sum_{i=1}^{m_\eta} \phi_i^\eta(\bar{x}) a_i^\eta \quad (35)$$

Where the  $\phi_i^p(\bar{x}), i \in \{1, \dots, m_p\}$ ,  $\phi_i^g(\bar{x}), i \in \{1, \dots, m_g\}$  and  $\phi_i^\eta(\bar{x}), i \in \{1, \dots, m_\eta\}$  are truncations of bases of the Hilbert space formed by the space  $\mathcal{L}_2(\Omega_f)$  of square integrable functions on  $\Omega_f$  equipped with the usual inner product  $\langle \cdot, \cdot \rangle_{\Omega_f}$ :

$$\langle f_1, f_2 \rangle_{\Omega_f} = \int_{\Omega_f} f_1 f_2 d\Omega \quad (36)$$

Orthonormality of the  $\phi_i^g(\bar{x})$  for the inner product (36) is assumed, as it is always possible to form an orthonormal basis from a non-orthonormal one using the Gram-Schmidt process [29]. Hence one has:

$$\langle \phi_i^g, \phi_j^g \rangle_{\Omega_f} = \delta_{ij} \quad \forall (i, j) \in \{1, \dots, m_g\}^2 \quad (37)$$

At this point, we only seek to obtain the form of our ROM. Hence, we just assume that the values of  $m_T, m_v, m_p, m_\eta, m_g$  are small.

## 4.2 Galerkin projections of governing equations

The ROM formulation is obtained by writing down Galerkin projections of:

- Momentum conservation eq.(17), accounting mass conservation eq.(1) via eq.(32);

- Poisson equation (19) for pressure;
- Equation (13) defining function  $g$ ;
- Equation (16) of the dynamic viscosity power-law model;
- Energy conservation equation (18).

For the sake of brevity, a short description of Galerkin projections, along with the introduction of boundary conditions, is given in section A.1 of the appendix, where equations are noted with an « A ». The resulting equations are (A.3), (A.7), (A.11), (A.22) (with  $b^\eta$  and  $b^g$  respectively defined in terms of  $a^\eta$  and  $a^g$  through equations (A.17) and (A.18)) and (A.25). In particular, section A.1.4 of the Appendix describes the Galerkin projection of the dynamic viscosity power-law model, with an original way to handle the issues caused by the pseudoplastic index  $n$ .

Let us suppose that space functions  $\bar{\phi}_i^v(\bar{x})$ ,  $i \in \{1, \dots, m_v\}$ ,  $\phi_i^p(\bar{x})$ ,  $i \in \{1, \dots, m_p\}$ , etc., are obtained through Proper Orthogonal Decomposition (POD) of simulated data (velocity, pressure, etc.). Then all elements (those with 3 indices, those with 2 indices and those with a single index) present in these equations, such as  $[M_{vp}]_{ki}$ ,  $[E_v]_{kij}$  and  $[M_{v\eta}]_{ki}$  in section A.1.1 for instance, could be computed. Coupled equations (A.3), (A.7), (A.11), (A.22) (along with equations (A.17) and (A.18)) and (A.25) would thus form a so-called “POD-Galerkin” ROM whose solutions would be small-size state vectors  $a^v$ ,  $a^p$ ,  $a^g$ ,  $a^\eta$  and  $a^T(t)$ .

However, in the frame of the Modal Identification Method (MIM) used in this paper, space functions are not obtained via POD. The literal form of elements such as  $[M_{vp}]_{ki}$ ,  $[E_v]_{kij}$ , etc., is not even taken into account. An optimization algorithm is used instead to build the ROM (see section 5.2). In order to reduce as much as possible the number of parameters to be identified in the ROM construction, further processing is performed in the following sections.

It is worth noticing that the case of several independent applied boundary conditions in the ROM formulation can be easily handled. For instance, the case of  $q$  heat flux densities  $\varphi_i(t)$ ,  $i \in \{1, \dots, q\}$ , would correspond to have  $\sum_{i=1}^q F_{\varphi_i}(\bar{x})\varphi_i(t)$  instead of  $F_\varphi(\bar{x})\varphi(t)$  in boundary condition (24), resulting in a  $\sum_{i=1}^q [V_{\varphi_i}]_k \varphi_i(t)$  term in equation (A.25). However, building such a ROM via an identification procedure requires heat flux signals and resulting temperature data representative of the system behavior. A ROM formulation for multiple internal heat sources can be handled in a similar manner.

### 4.3 Expression of nonlinear terms as matrix-vector products

In order to facilitate further operations, the first step consists to write the nonlinear terms as matrix-vectors products.

In equations (A.3), (A.7) and (A.25), these nonlinear terms are of the form  $\sum_{i=1}^{m_{v_1}} \sum_{j=1}^{m_{v_2}} [E]_{kij} a_i^{v_1} a_j^{v_2}$ , involving products of components of small-size state vectors  $a^{v_1}$  and  $a^{v_2}$  associated to two variables  $v_1$  and  $v_2$ .

Let us look at the case of the term  $\sum_{i=1}^{m_\eta} \sum_{j=1}^{m_\nu} [E_\nu]_{kij} a_i^\eta a_j^\nu$  in equation (A.3).

We define a bijection  $f$  allowing to define a global index  $q$  associated to indices  $i$  and  $j$ .

$$f : \begin{cases} \{1, \dots, m_\eta\} \times \{1, \dots, m_\nu\} \rightarrow \{1, \dots, m_\eta m_\nu\} \\ i, j \mapsto q = f(i, j) \end{cases}$$

We also define vector  $\Pi(a^\eta, a^\nu) \in \mathbb{R}^{m_\eta m_\nu}$  and matrix  $Q \in \mathbb{R}^{m_\nu \times m_\eta m_\nu}$  such that:

$$[\Pi(a^\eta, a^\nu)]_q = a_i^\eta a_j^\nu \quad \text{for } q = f(i, j), i \in \{1, \dots, m_\eta\}, j \in \{1, \dots, m_\nu\}$$

$$[Q_\nu]_{kq} = [E_\nu]_{kij} \quad \text{for } k \in \{1, \dots, m_\nu\}, q = f(i, j), i \in \{1, \dots, m_\eta\}, j \in \{1, \dots, m_\nu\}$$

Equation (A.3) can then be written as:

$$\sum_{i=1}^{m_p} [M_{vp}]_{ki} a_i^p + \sum_{q=1}^{m_\eta m_\nu} [Q_\nu]_{kq} [\Pi(a^\eta, a^\nu)]_q + Q_{in} \sum_{i=1}^{m_\eta} [M_{v\eta}]_{ki} a_i^\eta = 0 \quad \forall k \in \{1, \dots, m_\nu\}$$

The matrix-vector form writes:

$$M_{vp} a^p + Q_\nu \Pi(a^\eta, a^\nu) + Q_{in} M_{v\eta} a^\eta = 0 \quad (38)$$

In a similar way, equation (A.7) can be written as:

$$\sum_{i=1}^{m_p} [M_p]_{ki} a_i^p = \sum_{q=1}^{m_\eta m_\nu} [Q_p]_{kq} [\Pi(a^\eta, a^\nu)]_q \quad \forall k \in \{1, \dots, m_p\}$$

Where matrix  $Q_p \in \mathbb{R}^{m_p \times m_\eta m_\nu}$ . The matrix-vector form writes:

$$M_p a^p = Q_p \Pi(a^\eta, a^\nu) \quad (39)$$

in a similar manner, equation (A.25) can be written as:

$$\frac{da_k^T(t)}{dt} = \sum_{i=1}^{m_T} [M_T]_{ki} a_i^T(t) + \sum_{q=1}^{m_\nu m_T} [Q_{tr}]_{kq} [\Pi(a^\nu, a^T(t))]_q + \sum_{q=1}^{m_\eta m_g} [Q_{dv}]_{kq} [\Pi(a^\eta, a^g)]_q$$

$$+ [V_S]_k S(t) + [V_{int}]_k Q_{in} T_{in}(t) + [V_\varphi]_k \varphi(t) + [V_{ind}]_k T_{in}(t) + [V_w]_k T_w(t) \quad \forall k \in \{1, \dots, m_T\}$$

Where  $Q_{tr} \in \mathbb{R}^{m_T \times m_T m_\nu}$  et  $Q_{dv} \in \mathbb{R}^{m_T \times m_\eta m_g}$ . The matrix-vector form writes:

$$\begin{aligned} \frac{da^T(t)}{dt} &= M_T a^T(t) + Q_{tr} \Pi(a^\nu, a^T(t)) + Q_{dv} \Pi(a^\eta, a^g) \\ &+ V_S S(t) + V_{int} Q_{in} T_{in}(t) + V_\varphi \varphi(t) + V_{ind} T_{in}(t) + V_w T_w(t) \end{aligned} \quad (40)$$

In equation (A.11), the nonlinear term  $\sum_{i=1}^{m_\nu} \sum_{j=1}^{m_\nu} [E_g]_{kij} a_i^\nu a_j^\nu$  involves products of components of the same small-size state vector  $a^\nu$ . Some products in the sum are thus identical. Hence equation (A.11) can be written without repetition of identical products:

$$a_k^g = \sum_{i=1}^{m_v} \sum_{j=i}^{m_v} [F_g]_{kij} a_i^v a_j^v \quad \forall k \in \{1, \dots, m_g\} \quad (41)$$

With:

$$[F_g]_{kij} = \begin{cases} [E_g]_{kij} & \text{if } i = j \\ [E_g]_{kij} + [E_g]_{kji} & \text{if } i \neq j \end{cases} \quad i \in \{1, \dots, m_v\}, j \in \{i, \dots, m_v\}$$

Let us define a bijection  $f^*$  allowing to define a global index  $q$  associated to indices  $i$  and  $j$ .

$$f^* : \begin{cases} \{1, \dots, m_v\} \times \{i, \dots, m_v\} \rightarrow \left\{1, \dots, \frac{m_v(m_v + 1)}{2}\right\} \\ i, j \mapsto q = f^*(i, j) \end{cases}$$

We also define vector  $\Pi^*(a^v) \in \mathbb{R}^{\frac{m_v(m_v+1)}{2}}$  and matrix  $Q_g \in \mathbb{R}^{m_g \times \frac{m_v(m_v+1)}{2}}$  such that:

$$[\Pi^*(a^v)]_q = a_i^v a_j^v \quad \text{for } q = f^*(i, j), i \in \{1, \dots, m_v\}, j \in \{i, \dots, m_v\}$$

$$[Q_g]_{kq} = [F_g]_{kij} \quad \text{for } k \in \{1, \dots, m_g\}, q = f^*(i, j), i \in \{1, \dots, m_v\}, j \in \{i, \dots, m_v\}$$

Equation (41) can then be written as:

$$a_k^g = \sum_{q=1}^{\frac{m_v(m_v+1)}{2}} [Q_g]_{kq} [\Pi^*(a^v)]_q \quad \forall k \in \{1, \dots, m_g\}$$

The matrix-vector form writes:

$$a^g = Q_g \Pi^*(a^v) \quad (42)$$

#### 4.4 ROM for momentum conservation equation

It is shown in section A.2 of appendix that matrix  $M_p$  defined by (A.8) is invertible. Let us call  $[M_p]^{-1}$  its inverse. Equation (39) thus allows to obtain an expression of  $a^p \in \mathbb{R}^{m_p}$ :

$$a^p = [M_p]^{-1} Q_p \Pi(a^\eta, a^v) \quad (43)$$

Let us define matrix  $Q_{vp} \in \mathbb{R}^{m_v \times m_\eta m_v}$  such that:  $Q_{vp} = Q_v + M_{vp} [M_p]^{-1} Q_p$ .

Injecting equation (43) in equation (38) and taking into account the previous definition allows to « eliminate » the reduced state vector  $a^p$  associated to pressure from the momentum ROM equation. One gets:

$$Q_{vp} \Pi(a^\eta, a^v) + Q_{in} M_{v\eta} a^\eta = 0 \quad (44)$$

The term  $Q_{vp} \Pi(a^\eta, a^v)$  thus implicitly contains the pressure contribution.

## 4.5 ROM for viscosity model

The matrix-vector form of equation (A.22) writes:

$$M_{\eta\eta}b^\eta = W_{\eta\eta} + \ln(K)U_\eta + \left(\frac{n-1}{2}\right)(W_{\eta g} + M_{\eta g}b^g) \quad (45)$$

It is shown in section A.2 of appendix that matrix  $M_{\eta\eta}$  defined by (A.19) is invertible. Let us call  $[M_{\eta\eta}]^{-1}$  its inverse. Equation (A.21) shows that vector  $U_\eta$  is the first column of both matrices  $M_{\eta\eta}$  and  $M_{\eta g}$ . We can thus define  $V \in \mathbb{R}^{m_\eta}$  such as:

$$V = [M_{\eta\eta}]^{-1}U_\eta = \begin{bmatrix} 1 \\ 0 \\ \vdots \\ 0 \end{bmatrix} \quad (46)$$

In addition,  $M_{\eta g} \in \mathbb{R}^{m_\eta \times m_g}$  defined by equation (A.20) can be written as:

$$M_{\eta g} = [U_\eta \quad A_{\eta g}] \quad (47)$$

Where  $A_{\eta g} \in \mathbb{R}^{m_\eta \times (m_g - 1)}$ . Let us call:

$$A = [M_{\eta\eta}]^{-1}A_{\eta g} \in \mathbb{R}^{m_\eta \times (m_g - 1)} \quad (48)$$

Using (47), (46) and (48), one has:

$$[M_{\eta\eta}]^{-1}M_{\eta g} = [M_{\eta\eta}]^{-1}[U_\eta \quad A_{\eta g}] = [V \quad A] \in \mathbb{R}^{m_\eta \times m_g} \quad (49)$$

After performing the matrix-vector product of  $[M_{\eta\eta}]^{-1}$  with each term of equation (45), using equations (46) and (49) and defining elements  $V_\eta = [M_{\eta\eta}]^{-1}W_{\eta\eta} \in \mathbb{R}^{m_\eta}$  and  $V_g = [M_{\eta\eta}]^{-1}W_{\eta g} \in \mathbb{R}^{m_\eta}$ , one obtains:

$$b^\eta = V_\eta + \ln(K)V + \left(\frac{n-1}{2}\right)(V_g + [V \quad A]b^g) \quad (50)$$

Where  $b^\eta$  is linked to  $a^\eta$  by (A.17),  $b^g$  is linked to  $a^g$  by (A.18) and  $V = \begin{bmatrix} 1 \\ 0 \\ \vdots \\ 0 \end{bmatrix} \in \mathbb{R}^{m_\eta}$  (eq.(46)).

## 4.6 ROM for energy equation in modal form

Matrix  $M_T$  defined by equation (A.26) is symmetric. It is hence diagonalizable with real eigenvalues and its eigenvectors form an orthonormal basis of  $\mathbb{R}^{m_T}$ . Let us call  $D_T$  the diagonal matrix whose components are eigenvalues of  $M_T$  and  $P_T$  the orthogonal matrix ( $[P_T]^{-1} = [P_T]^T$ ) whose columns form a set of eigenvectors of  $M_T$ . One therefore has:

$$D_T = [P_T]^T M_T P_T \quad (51)$$

The following change of variable is now considered:

$$a^T(t) = P_T \tilde{a}^T(t) \quad (52)$$

It can be easily shown that the introduction of equation (52) in the vector of nonlinearities  $\Pi(a^v, a^T(t))$  of equation (40) yields:

$$\Pi(a^v, a^T(t)) = R\Pi(a^v, \tilde{a}^T(t)) \quad (53)$$

Where matrix  $R \in \mathbb{R}^{m_v m_T \times m_v m_T}$ .

We now define the following matrices and vectors:  $\tilde{Q}_{tr} = [P_T]^T Q_{tr} R$ ,  $\tilde{Q}_{dv} = [P_T]^T Q_{dv}$ ,  $B_S = [P_T]^T V_S$ ,  $B_{int} = [P_T]^T V_{int}$ ,  $B_\varphi = [P_T]^T V_\varphi$ ,  $B_{ind} = [P_T]^T V_{ind}$  and  $B_w = [P_T]^T V_w$ .

After introducing the change of variable (equation (52)) in equation (40), performing the matrix-vector product of  $[P_T]^{-1}$  ( $= [P_T]^T$ ) with each term of the equation and taking into account equation (51), equation (53) and previously defined elements, one obtains:

$$\begin{aligned} \frac{d\tilde{a}^T(t)}{dt} = & D_T \tilde{a}^T(t) + \tilde{Q}_{tr} \Pi(a^v, \tilde{a}^T(t)) + \tilde{Q}_{dv} \Pi(a^\eta, a^g) \\ & + B_S S(t) + B_{int} Q_{in} T_{in}(t) + B_\varphi \varphi(t) + B_{ind} T_{in}(t) + B_w T_w(t) \end{aligned} \quad (54)$$

#### 4.7 Output equation for specific observables

We are interested in some observable temperatures at specific locations  $\bar{x}_j$ ,  $j \in \{1, \dots, N_{obs}\}$  gathered in vector  $T_{obs} \in \mathbb{R}^{N_{obs}}$ . According to the temperature field approximation (27) and defining matrix  $C_{obs} \in \mathbb{R}^{N_{obs} \times m_T}$  such as  $[C_{obs}]_{ji} = \phi_i^T(\bar{x}_j) \quad \forall j \in \{1, \dots, N_{obs}\}, \forall i \in \{1, \dots, m_T\}$ , one has:

$$[T_{obs}]_j(t) = T(\bar{x}_j, t) = \sum_{i=1}^{m_T} \phi_i^T(\bar{x}_j) a_i^T(t) = \sum_{i=1}^{m_T} [C_{obs}]_{ji} a_i^T(t) \quad j \in \{1, \dots, N_{obs}\}$$

Which also writes in matrix form:

$$T_{obs}(t) = C_{obs} a^T(t)$$

Injecting equation (52) in the above equation and defining  $H = C_{obs} P_T \in \mathbb{R}^{N_{obs} \times m_T}$  leads to:

$$T_{obs}(t) = H \tilde{a}^T(t) \quad (55)$$

Other observable quantities can be defined as linear combinations of such primary observables (average temperature on some chosen area, for instance).

#### 4.8 Final form of the parametric thermo-rheological ROM of order $m$

Up to now, developments have been made considering that integers  $m_v, m_g, m_\eta$ , etc., are different, in order to keep some generality. However, in practice, all integers  $m_v, m_g, m_\eta$ , etc., are considered to be equal to a common integer  $m$ . In such case, matrix  $M_{v\eta}$  defined by (A.4) is also square ( $M_{v\eta} \in \mathbb{R}^{m \times m}$ ) and a similar reasoning to the one described in section A.2 of appendix allows showing that  $M_{v\eta}$  is invertible (using columns instead of rows). In equation

(44), matrix  $Q_{vp} \in \mathbb{R}^{m \times m^2}$ . After performing the matrix-vector product of  $[M_{v\eta}]^{-1}$  with each term of equation (44), one obtains the ROM for momentum equation:

$$Q'_{vp}\Pi(a^\eta, a^v) + Q_{in}a^\eta = 0 \quad (56)$$

Where  $Q'_{vp} = [M_{v\eta}]^{-1}Q_{vp} \in \mathbb{R}^{m \times m^2}$ .

The ROM associated with function  $g$  is equation (42) written for  $m_v = m_g = m$ :

$$a^g = Q_g\Pi^*(a^v) \quad (57)$$

Where  $Q_g \in \mathbb{R}^{m \times \frac{m(m+1)}{2}}$ .

The ROM associated with the viscosity model is given by equations (A.18), (50) and (A.17), written for  $m_\eta = m_g = m$ :

$$b_1^g = \ln(a_1^g); \quad b_i^g = \frac{a_i^g}{a_1^g} \quad \forall i \in \{2, \dots, m\} \quad (58)$$

$$b^\eta = V_\eta + \ln(K)V + \left(\frac{n-1}{2}\right)(V_g + [V \ A]b^g) \quad (59)$$

$$a_1^\eta = \exp(b_1^\eta); \quad a_i^\eta = b_i^\eta a_1^\eta \quad \forall i \in \{2, \dots, m\} \quad (60)$$

Where  $V_\eta \in \mathbb{R}^m$ ,  $V_g \in \mathbb{R}^m$ ,  $V = [1 \ 0 \ \dots \ 0]^T \in \mathbb{R}^m$  and  $A \in \mathbb{R}^{m \times (m-1)}$ .

The ROM for energy equation is equation (54) written for  $m_T = m_v = m_\eta = m_g = m$ :

$$\begin{aligned} \frac{d\tilde{a}^T(t)}{dt} &= D_T\tilde{a}^T(t) + \tilde{Q}_{tr}\Pi(a^v, \tilde{a}^T(t)) + \tilde{Q}_{dv}\Pi(a^\eta, a^g) \\ &+ B_S S(t) + B_{int}Q_{in}T_{in}(t) + B_\varphi\varphi(t) + B_{ind}T_{in}(t) + B_w T_w(t) \end{aligned}$$

Where  $D_T \in \mathbb{R}^{m \times m}$  is diagonal,  $\tilde{Q}_{tr} \in \mathbb{R}^{m \times m^2}$ ,  $\tilde{Q}_{dv} \in \mathbb{R}^{m \times m^2}$  and  $B_S, B_{int}, B_\varphi, B_{ind}$  and  $B_w$  are vectors of size  $m$ .

From now on, the following case is considered:

- At  $t = 0$ ,  $T_{in} = T_w = T_{init}$ ,  $\varphi = 0$  and  $S = 0$ , hence the initial temperature field is uniform, equal to  $T_{init}$ :  $T(\bar{x}, t = 0) = T_{init}$ ;
- For  $t > 0$ ,  $T_{in}$  and  $T_w$  remain constant and equal to  $T_{init}$  and  $\varphi$  remains equal to 0.

The ROM for energy equation thus comes down to:

$$\frac{d\tilde{a}^T(t)}{dt} = D_T\tilde{a}^T(t) + \tilde{Q}_{tr}\Pi(a^v, \tilde{a}^T(t)) + \tilde{Q}_{dv}\Pi(a^\eta, a^g) + B_S S(t) + B_{in}Q_{in} + B$$

Where  $B_{in} = B_{int}T_{init} \in \mathbb{R}^m$  and  $B = B_\varphi \underset{=0}{\varphi} + B_{ind}T_{init} + B_w T_{init} \in \mathbb{R}^m$ .

Furthermore, instead of using absolute temperature  $T(\bar{x}, t)$ , ROMs will be built for temperature deviation  $\delta T(\bar{x}, t)$  with respect to initial temperature  $T_{init}$ :

$$\delta T(\bar{x}, t) = T(\bar{x}, t) - T_{init}$$

It simply implies to set  $T_{init} = 0$  in the above ROM for energy equation ( $B_{in}$  and  $B$  are hence both equal to the null vector of size  $m$ ), which is thus written as follows:

$$\frac{d\tilde{a}^T(t)}{dt} = D_T \tilde{a}^T(t) + \tilde{Q}_{tr} \Pi(a^v, \tilde{a}^T(t)) + \tilde{Q}_{dv} \Pi(a^\eta, a^g) + B_S S(t) \quad (61)$$

In equations (56) to (61), vectors of nonlinearities are either of the form:

$$\Pi(a, b) = [a_1 b_1 \quad \cdots \quad a_1 b_m \quad a_2 b_1 \quad \cdots \quad a_2 b_m \quad \cdots \quad \cdots \quad a_m b_1 \quad \cdots \quad a_m b_m]^T \in \mathbb{R}^{m^2}$$

Or

$$\Pi^*(a) = [a_1^2 \quad a_1 a_2 \quad \cdots \quad a_1 a_m \quad a_2^2 \quad a_2 a_3 \quad \cdots \quad a_2 a_m \quad \cdots \quad a_{m-1}^2 \quad a_{m-1} a_m \quad a_m^2]^T \\ \in \mathbb{R}^{\frac{m(m+1)}{2}}$$

The output equation (55) written for  $m_T = m$  and for temperature deviations allows computing the observable deviation temperature vector  $\delta T_{obs} \in \mathbb{R}^{N_{obs}}$  from  $\tilde{a}^T(t) \in \mathbb{R}^m$ :

$$\delta T_{obs}(t) = H \tilde{a}^T(t) \quad (62)$$

Where  $H \in \mathbb{R}^{N_{obs} \times m}$ .

The parametric thermo-rheological ROM of order  $m$  is thus formed by equations (56) to (62), allowing the computation of reduced state vectors  $a^v, a^\eta, a^g$  and  $\tilde{a}^T(t)$  of size  $m$  as a function of parameters  $K, n, Q_{in}$  and applied heat source power  $S(t)$ .

## 4.9 Numerical resolution of ROM equations

First of all, let us consider the initial instant. At time  $t = 0$ , the fluid is motionless and the temperature field is uniform:  $T(\bar{x}, t = 0) = T_{init}$ , i.e.  $\delta T(\bar{x}, t = 0) = 0$ . Corresponding ROM state vectors are thus as follows:

- $a^v = [0]$  (null vector of size  $m$ ) so that  $\bar{v}(\bar{x}, t = 0) = \bar{0}$ ;
- So, according to Eq.(57),  $a^g = [0]$  which allows verifying  $g(\bar{x}, t = 0) = 0$ ;
- Since  $a^g = [0]$ , Eq.(58), and consequently, equations (59) and (60), cannot be solved and  $a^\eta$  cannot be determined. However, this is not important as Eq.(56) is verified at  $t = 0$  whatever  $a^\eta$  because  $a^v = [0]$  and  $Q_{in} = 0$ .
- Since  $a^v = a^g = [0]$ ,  $\frac{d\tilde{a}^T}{dt} = [0]$  and  $S = 0$ , Eq.(61) writes  $D_T \tilde{a}^T = [0]$ , hence  $\tilde{a}^T = [0]$ , which leads to  $\delta T_{obs}(t = 0) = 0$  according to equation (62).

The problem is then considered as quasi-static for the fluid flow and unsteady for the thermal state: as soon as  $t > 0$ , fields of velocity, function  $g$  and dynamic viscosity reach instantaneously their respective steady states  $\bar{v}(\bar{x}), g(\bar{x}), \eta(\bar{x})$ , whereas  $\delta T(\bar{x}, t)$  starts to vary, because of two source terms in the energy equation (18):

- Viscous dissipation term  $\frac{\eta g}{\rho c_p}$ ; this term depends on  $\eta$  and  $g$ , and thus on  $K, n, Q_{in}$ . It is constant for  $t > 0$  and hence acts as a step source term.

- Volumetric heat power term  $\frac{\chi_s}{\rho C_p} S(t)$ .

Coupled equations (56) to (60), parametrized by  $K, n, Q_{in}$ , form the ROM associated to the stationary fluid flow. As the flow is assumed quasi-static, these equations are solved first.

In order to ensure that  $a_1^g > 0$ , which is mandatory to compute  $b_1^g = \ln(a_1^g)$  in Eq.(58), constraints on matrix  $Q_g \in \mathbb{R}^{m \times \frac{m(m+1)}{2}}$  in Eq. (57) are introduced: components of the first line of  $Q_g$  are all set to zero except for those multiplying components  $(a_i^v)^2$  in  $\Pi^*(a^v)$ , which are forced to be  $> 0$ .

For order 1 ROM, Eq.(56) writes:

$$Q'_{vp} a^\eta a^v + Q_{in} a^\eta = 0$$

Where  $Q'_{vp}$ ,  $a^\eta$  and  $a^v$  are simple scalars. As  $a^\eta$  has to be non-zero, one has  $a^v = -\frac{Q'_{vp}}{Q_{in}}$ .

Equation (57) then allows to compute  $a^g$ . Equations (58) to (60) then allow to compute  $a^\eta$ .

One should note that for order 1 ROM,  $a^v$  does not depend on  $a^\eta$  and hence does not depend on viscosity parameters  $K$  and  $n$ . This shows that the order 1 ROM is intrinsically biased. Such bad feature will not appear anymore in ROMs of order higher than 1.

For ROMs of order  $m > 1$ , coupled equations (56) to (60) have to be solved iteratively. One possible way is to first consider a simplified equation (56) composed of scalar equations similar to equation (56) for order 1 ROM, in order to compute an initial guess for vector  $a^v \in \mathbb{R}^m$ . Then equation (57) is used to compute  $a^g$  and equations (58) to (60) then give  $a^\eta$ . An iterative loop is then performed on equations (56) to (60) using the complete equation (56), until convergence on residues of these equations is obtained.

Once equations (56) to (60) are solved, state vectors  $a^v, a^\eta, a^g$  of size  $m$ , corresponding to the steady flow, are obtained. Then the ROM for energy equation given by equation (61) can be solved to compute  $\tilde{a}^T(t) \in \mathbb{R}^m$ . For a given fluid, i.e. given viscosity parameters  $K$  and  $n$ , and a given flowrate  $Q_{in}$ , equation (61) is linear with respect to  $\tilde{a}^T(t)$ .

The transport term  $\tilde{Q}_{tr} \Pi(a^v, \tilde{a}^T(t))$  in Eq. (61) can be written as follows:

$$\tilde{Q}_{tr} \Pi(a^v, \tilde{a}^T(t)) = M(a^v) \tilde{a}^T(t)$$

Where matrix  $M(a^v) \in \mathbb{R}^{m \times m}$  is defined by:

$$[M(a^v)]_{i,j} = \sum_{k=1}^m [\tilde{Q}_{tr}]_{i,(k-1)m+j} [a^v]_k \quad \forall i \in \{1, \dots, m\}, \forall j \in \{1, \dots, m\}$$

Matrix  $A(a^v) \in \mathbb{R}^{m \times m}$  is defined as  $A(a^v) = D_T + M(a^v)$

Equation (61) can thus be written as:

$$\frac{d\tilde{a}^T(t)}{dt} = A(a^v) \tilde{a}^T(t) + \tilde{Q}_{av} \Pi(a^\eta, a^g) + B_s S(t)$$

Such linear time invariant (LTI) system can be solved directly at each time step using an implicit Euler integration scheme. This is done by standard LAPACK routine DGESV.

## 4.10 Typical usages of ROMs

ROMs are useful for handling different tasks, especially those requiring many queries to the model, for which their small size allows saving computing time.

Because parameters  $K, n, Q_{in}$  and heat source power signal  $S(t)$  appear explicitly in the ROM equations (56) to (62), ROMs can be used for parametric studies.

In addition, the ROM equations (56) to (62) can be analytically differentiated with respect to viscosity parameters  $K$  and  $n$  to obtain a ROM for computing vectors of sensitivities  $\frac{\partial \delta T_{obs}}{\partial K}$  and  $\frac{\partial \delta T_{obs}}{\partial n}$  for different values of the parameters, thus allowing to get valuable information prior to the estimation of  $K$  and  $n$ .

Of course, ROMs can be used for solving the inverse problem for on-line estimation of  $K$  and  $n$  during a process. If a gradient-based method is used, the objective function is quickly computed using the ROM equations (56) to (62) and the gradient of the objective function can be computed either by numerical differentiation or by using the ROM for sensitivities mentioned above.

It is also possible to linearize the ROM equations (56) to (62) around chosen nominal values of  $K, n, Q_{in}$  to obtain a linearized ROM parametrized by deviations  $\delta K, \delta n, \delta Q_{in}$  with respect to nominal values of parameters. Such a linearized ROM could be then used for on-line estimation of small modifications of a polymer during a process.

## 5 Data generation and ROMs identification

Vector functions  $\tilde{a}^T(t)$  and  $\delta T_{obs}(t)$  depend on parameters  $K, n, Q_{in}$ . In the ROM identification process, notations  $\tilde{a}^T(j, t)$  and  $\delta T_{obs}(j, t)$  correspond respectively to the vector functions  $\tilde{a}^T(t)$  and  $\delta T_{obs}(t)$  associated with a particular triplet  $(K, n, Q_{in})_j$ .

### 5.1 Data generation

The identification of the ROM constitutive parameters requires some input-output data:

- a chosen heat source power signal  $S^{data}(t)$ , corresponding in practice to discrete values  $S^{data}(t_k), k \in \{1, \dots, N_t^{id}\}$ , as well as a set of triplets  $(K, n, Q_{in})_j^{data}, j \in \{1, \dots, N_s^{id}\}$ ;

- the resulting temperature deviations  $[\delta T_{obs}^{FOM,data}]_i(j, t_k)$ ,  $i \in \{1, \dots, N_{obs}\}$ ,  $j \in \{1, \dots, N_s^{id}\}$ ,  $k \in \{1, \dots, N_t^{id}\}$ . In the present work, temperature data are computed with the Finite Elements full order model briefly presented in section 6.1.

## 5.2 ROMs identification

### 5.2.1 Optimization problem for the order $m$ ROM

In order to effectively build a ROM of order  $m$ , elements of its constitutive matrices and vectors need to be computed. In the framework of the Modal Identification Method, these elements are identified through an algorithm using optimization techniques. The ROM construction is therefore recast into a parameter estimation problem. Parameters to be identified are components of:

- $Q'_{vp} \in \mathbb{R}^{m \times m^2}$ ,  $Q_g \in \mathbb{R}^{m \times \frac{m(m+1)}{2}}$ ,  $V_\eta \in \mathbb{R}^m$ ,  $V_g \in \mathbb{R}^m$ ,  $A \in \mathbb{R}^{m \times (m-1)}$ ,  $D_T \in \mathbb{R}^{m \times m}$  diagonal,  $\tilde{Q}_{tr} \in \mathbb{R}^{m \times m^2}$ ,  $\tilde{Q}_{dv} \in \mathbb{R}^{m \times m^2}$  and  $B_S \in \mathbb{R}^m$ , in equations (56) to (61),  $V = [1 \ 0 \ \dots \ 0]^T \in \mathbb{R}^m$  being known;
- $H \in \mathbb{R}^{N_{obs} \times m}$  in output equation (62).

However, as mentioned in section 4.9, only  $m$  components in the first line of matrix  $Q_g$  are non-zero. For a given order  $m$ , the number of unknown parameters is hence:

$$N_{param}(m) = 3m^3 + \frac{(m-1)m(m+1)}{2} + m^2 + 4m + N_{obs}m$$

Except for components of matrix  $H$ , unknown parameters to be identified are gathered into vector  $\theta$  of size  $N_\theta(m) = 3m^3 + \frac{(m-1)m(m+1)}{2} + m^2 + 4m$ .

All parameters are identified through the minimization of a functional  $\mathcal{J}_{ident}^{(m)}(\theta, H)$  based on the quadratic deviation between:

- the temperature  $[\delta T_{obs}^{ROM}]$  computed with the ROM on the one hand (hence depending on  $\theta$  and  $H$ ), and
- the corresponding temperature data  $[\delta T_{obs}^{FOM,data}]$ , computed here with the reference full order model (FOM) on the other hand,

for the same applied heat source signal  $S^{data}(t_k)$ ,  $k \in \{1, \dots, N_t^{id}\}$  and the same set of triplets  $(K, n, Q_{in})_j^{data}$ ,  $j \in \{1, \dots, N_s^{id}\}$ .

For a given order  $m$ , the quadratic functional  $\mathcal{J}_{ident}^{(m)}(\theta, H)$  therefore writes:

$$\mathcal{J}_{ident}^{(m)}(\theta, H) = \sum_{i=1}^{N_{obs}} \sum_{j=1}^{N_s^{id}} \sum_{k=1}^{N_t^{id}} \left( [\delta T_{obs}^{ROM}]_i(j, t_k, \theta, H) - [\delta T_{obs}^{FOM,data}]_i(j, t_k) \right)^2 \quad (63)$$

In order to assess the quality of the identified ROM, the mean quadratic discrepancy  $\sigma_{ident}^{(m)}$  (in  $K$ ) between data from FOM and corresponding values computed by ROM is computed:

$$\sigma_{ident}^{(m)} = \sqrt{\frac{\mathcal{J}_{ident}^{(m)}(\theta, H)}{N_{obs} N_s^{id} N_t^{id}}} \quad (64)$$

### 5.2.2 Identification procedure for ROM of order $m$

Equations (56) to (62) show that ROM outputs  $\delta T_{obs}$  have nonlinear dependency on matrices and vectors whose components are gathered in  $\theta$ , whereas they depend linearly on  $H$ . As a consequence, two types of optimization methods are used for the minimization of  $\mathcal{J}_{ident}^{(m)}(\theta, H)$  through a two-step approach. Both optimization algorithms are briefly described in section A.3 of the appendix. A nonlinear iterative method is employed for the estimation of vector  $\theta$ . A Particle Swarm Optimization (PSO) algorithm [20] has been used in the present work (cf. section A.3.1 of appendix). At each iteration of the PSO algorithm, matrix  $H$  is computed via Ordinary Least Squares (cf. section A.3.2 of appendix).

Figure 2 gives the identification procedure for a ROM of given order  $m$  in the Modal Identification Method. The stopping criterion is usually based on the fact that  $\sigma_{ident}^{(m)}$  does not decrease for a large number of successive iterations.

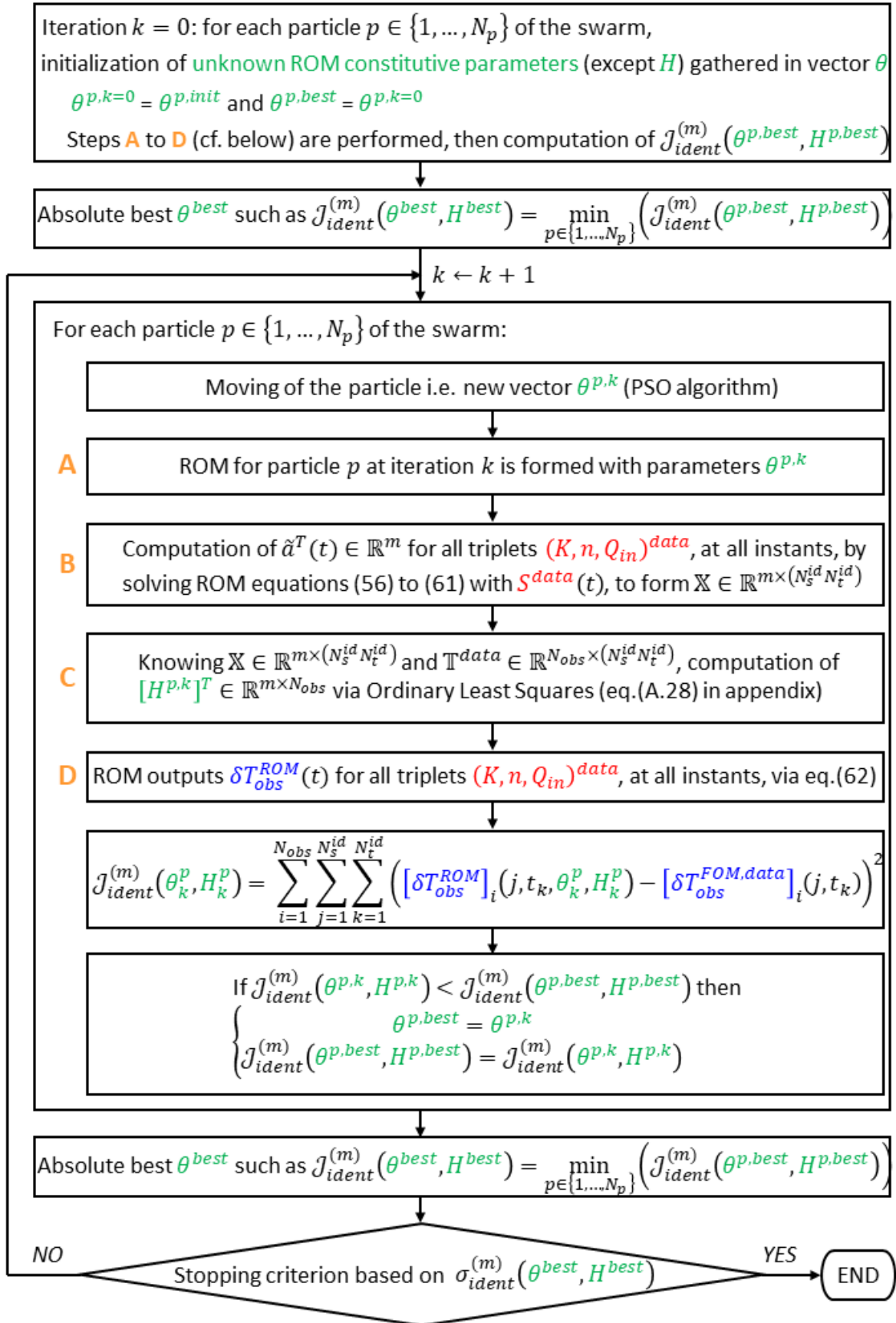


Figure 2. Summary of the identification procedure for a ROM of given order  $m$

### 5.2.3 The global procedure for building a series of ROMs of successive orders

First of all  $J_{ident}^{(1)}(\theta, H)$  is minimized in order to obtain  $\theta$  and  $H$  associated with a single term in approximation of variables (equations (27), (30), (33), (34), (35)) and thus defining a ROM of order  $m = 1$ . A ROM of order  $m = 2$  is then built by minimizing  $J_{ident}^{(2)}(\theta, H)$  which leads to larger  $\theta$  and  $H$  associated with two terms in approximation of variables. ROMs of higher order are then built successively by incrementing order  $m$  and minimizing corresponding functional  $J_{ident}^{(m)}(\theta, H)$  until a predefined stopping criterion is satisfied. The global procedure is summarized as follows:

1.  $m \leftarrow 1$
2. Minimization of  $J_{ident}^{(1)}(\theta, H)$ : identification of  $\theta, H$  for order 1 ROM
3.  $m \leftarrow m + 1$
4. Minimization of  $J_{ident}^{(m+1)}(\theta, H)$ : identification of new  $\theta, H$  for order  $m + 1$  ROM
5. Test of stopping criterion: 2 possibilities:
  - 5.1 if  $\sigma_{ident}^{(m+1)} \approx \sigma_{ident}^{(m)}$  then STOP else go to 3
  - 5.2 if  $\sigma_{ident}^{(m)}$  reaches the wished accuracy, then STOP else go to 3

As vector  $\theta$  is estimated via an iterative method (here PSO), an initial guess for  $\theta$  is required.

As matrix  $H$  is computed by Ordinary Least Squares at each iteration of the PSO algorithm, no initial guess is needed for  $H$ .

For  $m=1$ , components of  $\theta$  are randomly initialized.

When identifying the order  $m + 1$  ROM ( $m \geq 1$ ), the components of  $\theta$  in the order  $m$  ROM previously identified are used as initial guesses for the corresponding unknown components of  $\theta$  in the order  $m + 1$  ROM. In order to ensure this initial  $m + 1$  ROM gives the same solutions as the order  $m$  ROM, the other parameters are initially set to zero, except for the following ones which are required to be non-zero so that the set of equations can be solved: the component  $Q'_{vp}$  of indices  $(m + 1, (m + 1)^2)$  and the  $(m + 1)^{th}$  component of both  $V_\eta$  and  $D_T$ , the latter being  $< 0$ . The functional  $J_{ident}^{(m+1)}(\theta, H)$  to be minimized hence starts from the value obtained for  $J_{ident}^{(m)}(\theta, H)$  and then decreases throughout iterations.

The series of ROMs of order 1 to  $m_{max}$  ( $m_{max}$  depending on the stopping criterion) is therefore built recursively, the ROM of order  $m \geq 1$  being used to start the identification of the ROM of order  $m + 1$ . The ROM of order  $m$  is neither a truncation of the ROM of order  $m + 1$  nor a truncation of the ROM of order  $m_{max}$ .

## 5.3 Comments on ROMs construction and possible extensions

### 5.3.1 Other data sets

If one wants to use other data sets (observable temperatures, triplets  $(K, n, Q_{in})$ , time sampling), the procedure for ROMs construction has to be done again. Of course, the ROMs already built can be used to speed up the process. For instance, the components of vector  $\theta$  in an order  $m$  ROM can be used as initial values for building a new ROM of same order for the new data set. No initial guess is needed for output matrix  $H$ , which is computed at each iteration of the PSO algorithm, possibly for another set of observable temperatures.

### 5.3.2 Other geometries and parameters $\lambda, \rho, C_p$

Although the ROM general form (equations (56) to (62)) is the same whatever the geometry, the ROMs construction depends on temperature data which depend on the problem geometry and on values of parameters  $\lambda, \rho, C_p$  in both fluid and solid parts. Therefore, ROMs are built for a given geometry and a given set of  $\lambda, \rho, C_p$  values. For another geometry and/or other values of  $\lambda, \rho, C_p$ , the procedure for ROMs construction has to be done again. ROMs already built can be used as initial guesses, obviously with less benefit than in the case of section 5.3.1, especially if geometry changes.  $\lambda, \rho, C_p$  in both fluid and solid parts could become explicit parameters in the ROMs, just as  $(K, n, Q_{in})$ , by adjusting the ROMs equations and constructing ROMs with temperature data sets obtained for different values of  $\lambda, \rho, C_p$ .

### 5.3.3 Extension to other viscosity models

ROMs for other viscosity models can be developed by replacing equations (58) to (60) by new equations corresponding to the chosen viscosity model. The other ROM equations (56), (57), (61) and (62) remain unchanged, thus allowing easy extensions of the whole ROM formulation. In particular, the approach developed in section A.1.4 of the Appendix to handle the issue of the pseudoplastic index  $n$  acting as an exponent in the power-law model (15), can be used for more complex viscosity models, such as “Cross fluid” [26] and “Carreau fluid” [27] models for instance. Of course, temperature data sets for different values of the viscosity parameters of the chosen model should be used for the ROMs construction. Components of vector  $\theta$  in equations (56), (57), (61) and (62) of an existing order  $m$  ROM based on the power-law model can be used as initial values for building ROMs of same order based on other viscosity models.

## 6 Application: laminar polymer flow in annular duct

### 6.1 The considered configuration and the reference model

#### 6.1.1 Problem description

Figure 3 describes an annular axial laminar flow problem in an axisymmetric cylindrical coordinate system. The solid domain is  $\Omega_s = \Omega_{s,1} \cup \Omega_{source} \cup \Omega_{s,2}$ , where  $\Omega_{s,1}$  corresponds to

the outer part of the central axis,  $\Omega_{\text{source}}$  corresponds to the inner part of the central axis which contains an heat source delivering a time-varying volumetric power  $S(t)$ , and  $\Omega_{s,2}$  corresponds to the outer wall of thickness  $e$ .  $L$  is the length of the annular part. The polymer (domain  $\Omega_f$ ) enters the duct at  $z = -L'$  and is guided to the annular part by a  $45^\circ$  cone. For  $z \geq 0$ , the polymer flows between the outer radius  $R$  and the inner radius  $\kappa R$ .  $\xi R$  is the position in the radial direction where shear rate is zero (maximum velocity). Although it is possible to describe the problem only for  $z \geq 0$ , modeling the cone on the upstream side allows us to avoid arbitrary assumption on the thermal boundary condition at the central axis for  $z = 0$ .

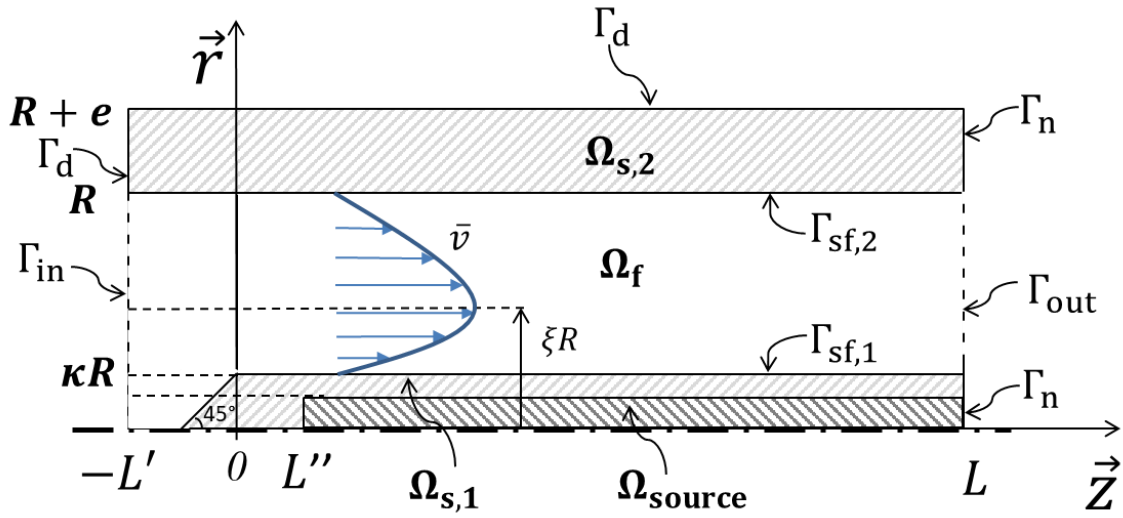


Figure 3 : Illustration of the annular flow problem

The present physical problem is described accurately by conservation equations (1), (17) and (18) as well as equations (13) and (16).

Boundary conditions are set within the frame described in section 2.2.

On the flow inlet  $\Gamma_{\text{in}}$  ( $z = -L', r \in [0, R]$ ), the flowrate and the temperature are fixed:  $Q = Q_{\text{in}}$  (special form of Eq.(20)) and  $T = T_{\text{in}} = T_{\text{init}}$  (special form of Eq.(21)), with  $T_{\text{init}}$  the initial uniform temperature of the system.

On the flow outlet  $\Gamma_{\text{out}}$  ( $z = L, r \in ]\kappa R, R[$ ), both equations (22) and (23) are used.

On  $\Gamma_n$  ( $z = L, r \in [0, \kappa R] \cup [R, R + e]$ ), a Neumann homogeneous condition is applied (special form of Eq.(24) with  $\varphi = 0$ ).

On  $\Gamma_d$  ( $z = 0, r \in [R, R + e]$  and  $z \in [-L', L], r = R + e$ ), we set  $T = T_w = T_{\text{init}}$  (special form of Eq.(25)).

The no-slip condition (26) is applied on  $\Gamma_{\text{sf}} = \Gamma_{\text{sf},1} \cup \Gamma_{\text{sf},2}$  where  $\Gamma_{\text{sf},1}$  is the surface of the central axis ( $z \in [0, L], r = \kappa R$  and  $z \in [-\kappa R, 0], r = \kappa R + z$ ) and  $\Gamma_{\text{sf},2}$  is the surface inside the channel at radius  $R$  ( $z \in [-L', L], r = R$ ). Continuity of temperature and heat flux density is assumed across the fluid/solid interfaces.

### 6.1.2 Numerical methods and parameters

The software « ANSYS® POLYFLOW® » is used to simulate our axisymmetric model. The mesh grid, presented in Figure 4, is composed of 16,218 nodes and 15,946 linear quadrilateral elements. The sizes of the elements are less than 2 mm and refined at the intersections of domains or near the section change area of the flow.

Picard iteration [30] and Crank-Nicolson method [31] are used for solving our nonlinear flow equations and thermal transient problem. The initial time step is set to 0.001 s. The largest calculation time step is less than 0.1 s, with an initial time value  $t_0 = 0$  s and an upper time limit  $t_{final}$  ranging from 40 to 60 s.

The « ANSYS® POLYFLOW® » model is called our full order model (FOM) in the following.

The geometric parameters are chosen according to an actual experimental lab device:  $L = 76$  mm,  $L' = 14$  mm,  $e = 20$  mm,  $R = 10$  mm and  $\kappa = 0.4$ . The material of the solid domains  $\Omega_{s,1}$  and  $\Omega_{s,2}$  is stainless steel with a thermal conductivity  $\lambda_s = 15 \text{ W.m}^{-1}.\text{K}^{-1}$ , a density  $\rho_s = 7900 \text{ kg.m}^{-3}$  and a specific heat capacity  $C_{p_s} = 500 \text{ J.kg}^{-1}.\text{K}^{-1}$ . Specific values are used for the region  $\Omega_{source}$  ( $z > L' = 6$  mm and  $r < 2.1$  mm) of the central axis which is instrumented (heat source, thermocouples' wires, epoxy resin):  $\lambda_s = 0.6 \text{ W.m}^{-1}.\text{K}^{-1}$ ,  $\rho_s = 1231 \text{ kg.m}^{-3}$  and  $C_{p_s} = 1159 \text{ J.kg}^{-1}.\text{K}^{-1}$ . The properties of Polypropylene are used for the polymer flow domain  $\Omega_f$ :  $\lambda_f = 0.23 \text{ W.m}^{-1}.\text{K}^{-1}$ ,  $\rho_f = 900 \text{ kg.m}^{-3}$  and  $C_{p_f} = 2800 \text{ J.kg}^{-1}.\text{K}^{-1}$ . Temperature  $T_{in} = T_w = T_{init}$  is set to 473.15 K.

Five virtual thermocouples  $[T_{obs}]_i$ ,  $i \in \{1; 5\}$ , are considered:  $[T_{obs}]_1$  is located at ( $z = -4$  mm,  $r = 0$ ) whereas  $[T_{obs}]_2$  to  $[T_{obs}]_5$  are positioned on the surface of the central axis ( $r = \kappa R$ ) from  $z = 6$  mm to  $z = 34$  mm with equidistance between them (cf. Figure 4).

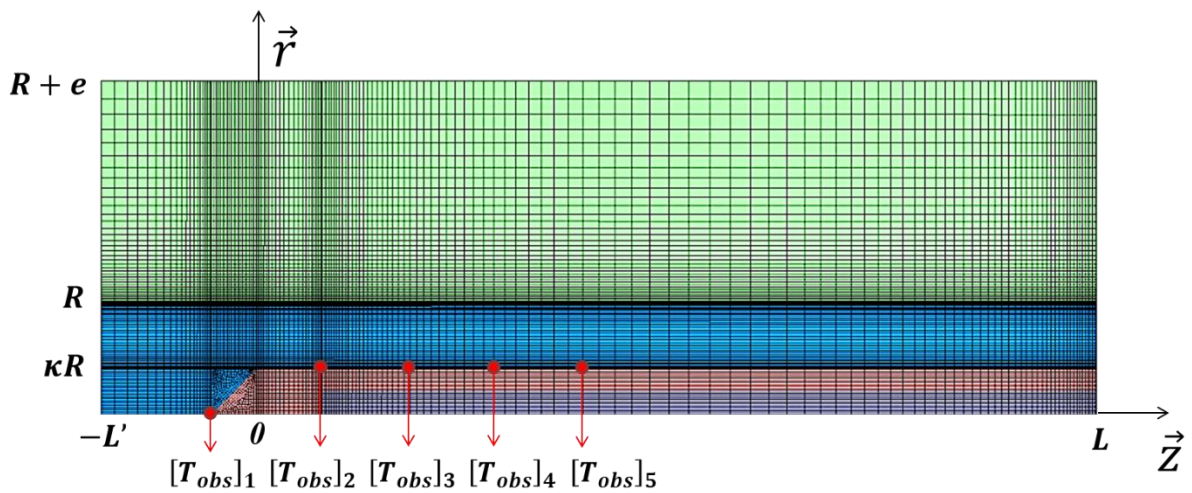


Figure 4 : Mesh grid and position of virtual thermocouples  $[T_{obs}]_i$ ,  $i \in \{1; 5\}$

## 6.2 Identification of a series of ROMs

First of all, it is worth noticing that although the general form of the ROMs equations is independent of the geometry, ROMs are built using data simulated for a given geometric configuration. For other geometries, ROMs of similar form but with different parameter values need to be built from new data.

Instead of a Cartesian regular mesh of the  $(K, n, Q_{in})$  parameter space, an Improved Hypercube Sampling (IHS) approach [32] has been used in order to cover the space with a limited number of  $(K, n, Q_{in})$  triplets. Using IHS the coordinates in the parameters space are regularly spaced out but the set is formed so that any two distinct  $(K, n, Q_{in})$  triplets do not share a common  $K$ ,  $n$  or  $Q_{in}$  value and in such way that the parameter space is covered as uniformly as possible. Chosen ranges of parameter values are  $K \in ]2000; 35000[$  Pa.s<sup>n</sup>,  $n \in ]0.33; 0.50[$  and  $Q_{in} \in ]10; 120[$  cc.s<sup>-1</sup> [33].

Computations were performed for 100 triplets  $(K, n, Q_{in})$ , however convergence was not obtained for two of them. The input data for the identification of a series of ROMs are therefore the set of  $N_s^{id} = 98$  triplets  $(K, n, Q_{in})$  depicted by red dots in Figure 5.

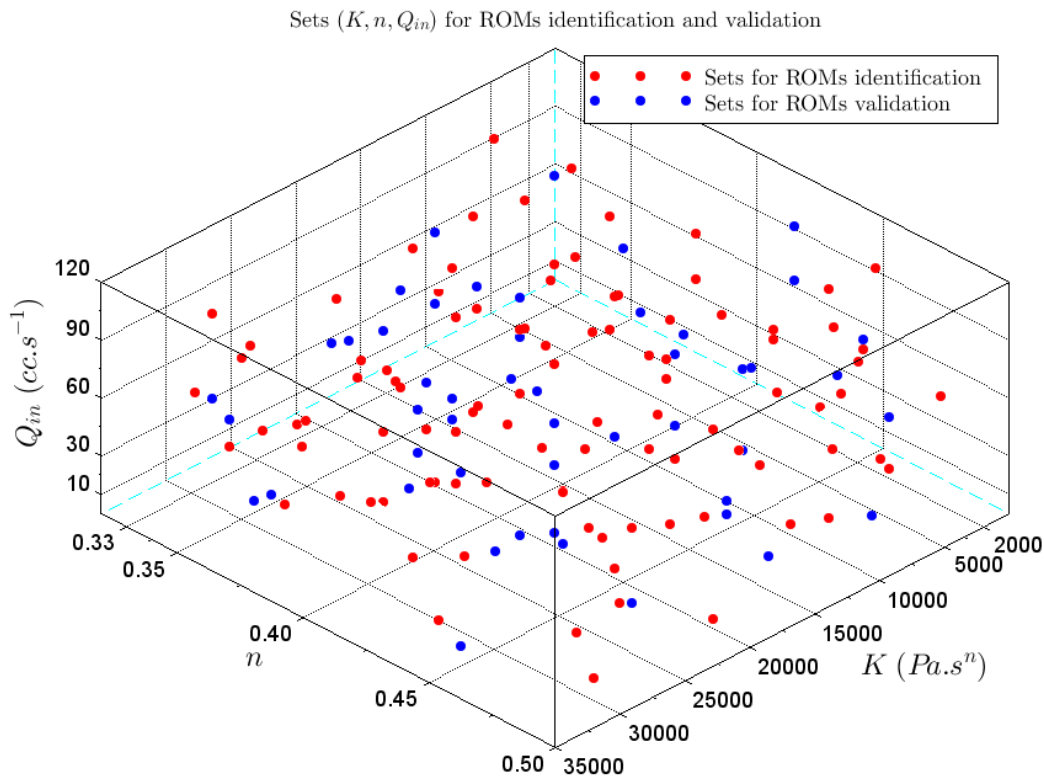


Figure 5. triplets  $(K, n, Q_{in})$  used for ROMs identification and validation.

Two heat source terms act simultaneously on the temperature distribution inside the system:

- the viscous dissipation term:  $\frac{\eta g}{\rho c_p}$  in energy conservation equation (18) and its counterpart  $\tilde{Q}_{dv}\Pi(a^\eta, a^g)$  in ROM' equation (61). This term is of course different for any given triplet  $(K, n, Q_{in})$ . As the flow is assumed to be steady (quasi-static flow assumption), this term does not depend on time.
- the applied heat source power:  $\frac{\chi_S}{\rho c_p} S(t)$  in energy conservation equation (18) and its counterpart  $B_S S(t)$  in ROM' equation (61). This term is the same whatever the triplet  $(K, n, Q_{in})$  but may vary with time.

As mentioned in section 4.9, for a given fluid, i.e. given viscosity parameters  $K$  and  $n$ , and a given flowrate  $Q_{in}$ , equation (61) is linear with respect to  $\tilde{a}^T(t)$ . According to linearity, the superposition principle allows to build ROMs by activating each source term separately. However, only the power heat source term  $B_S S(t)$  can of course be turned off.

Therefore, in order to decouple the influence of each heat source term, temperature data used for ROMs identification come from two different problems:

- viscous dissipation only, i.e. no applied heat power ( $S(t) = 0$ );
- viscous dissipation and applied heat power simultaneously. For a given triplet  $(K, n, Q_{in})$ , the linearity of equation (61) with respect to  $\tilde{a}^T(t)$  allows to use a step signal  $S^*(t)$  as heat power signal (here of magnitude  $8 \times 10^6$  W.m<sup>-3</sup>) for the ROMs identification.

For each problem, initial temperature  $T_{init}$  is set to 473.15 K.

The outputs are the temperature deviations  $\delta T_{obs}(t)$  at the 5 virtual thermocouples  $[T_{obs}]_i$ ,  $i \in \{1; 5\}$  shown in Figure 4 (we thus have  $N_{obs} = 5$ ).

The functional  $\mathcal{J}_{ident}^{(m)}$  to be minimized for the ROMs construction is therefore given by:

$$\mathcal{J}_{ident}^{(m)} = \mathcal{J}_{ident}^{(m),S=0} + \mathcal{J}_{ident}^{(m),S=S^*}$$

Where  $\mathcal{J}_{ident}^{(m),S=0}$  and  $\mathcal{J}_{ident}^{(m),S=S^*}$  are respectively related to the “ $S(t) = 0$ ” and “ $S(t) = S^*(t)$ ” problems and have both the form of Eq.(63). One has  $N_t^{id,S=0} = N_t^{id,S=S^*} = 601$ . The total number of instants for  $\mathcal{J}_{ident}^{(m)}$  is thus  $N_t^{id} = N_t^{id,S=0} + N_t^{id,S=S^*} = 1202$ .

A series of ROMs of order  $m = 1$  to 8 has been constructed by applying the identification procedure described in section 5.2 and using these input-output data. The value of the mean quadratic error  $\sigma_{ident}^{(m)}$  between FOM and ROM, defined by Eq.(64), is shown in Figure 6 as a function of ROM order  $m$  (red curve). As expected,  $\sigma_{ident}^{(m)}$  decreases with the order  $m$ , down to 0.024 K for  $m = 8$ . ROMs of higher orders did not lead to further improvement.

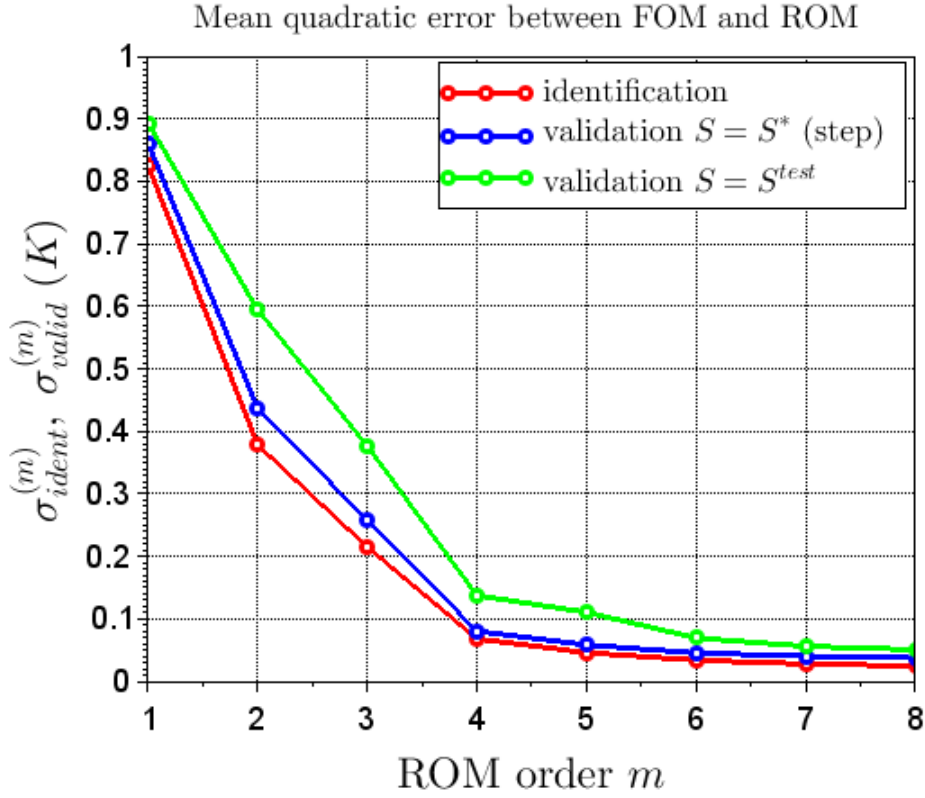


Figure 6. ROMs identification and validation tests: mean quadratic errors  $\sigma_{ident}^{(m)}$  and  $\sigma_{valid}^{(m)}$  between FOM and ROM as a function of ROM order  $m$ .

In addition, some examples of evolutions of temperature deviations are shown in Figure 7 for 2 triplets in the case  $S(t) = 0$  and in Figure 8 for 2 other triplets in the case  $S(t) = S^*(t)$  (step signal of magnitude  $8 \times 10^6 \text{ W.m}^{-3}$ ). The graphs in both figures assess the ability of the identified order 8 ROM to reproduce the FOM outputs. Dynamics and temperature magnitude are different depending on the triplet  $(K, n, Q_{in})$ .

In addition to the global quantity  $\sigma_{ident}^{(m)} = \sqrt{\frac{J_{ident}^{(m)}}{5 \times 98 \times 1202}}$  (Eq.(64)), the quantity  $\sigma_{ident,set}^{(m)}(j), j \in \{1, \dots, 98\}$ , related to each triplet  $(K, n, Q_{in})$ , is defined for each heat source case:

$\forall j \in \{1, \dots, 98\}$ :

$$\sigma_{ident,set}^{(m),S=0}(j) = \sqrt{\frac{\sum_{i=1}^{N_{obs}} \sum_{k=1}^{N_t^{id}} \left( [\delta T_{obs}^{ROM,S=0}]_i(j, t_k) - [\delta T_{obs}^{FOM,data,S=0}]_i(j, t_k) \right)^2}{5 \times 601}}$$

and

$$\sigma_{ident,set}^{(m),S=S^*}(j) = \sqrt{\frac{\sum_{i=1}^{N_{obs}} \sum_{k=1}^{N_t^{id}} \left( [\delta T_{obs}^{ROM,S=S^*}]_i(j, t_k) - [\delta T_{obs}^{FOM,data,S=S^*}]_i(j, t_k) \right)^2}{5 \times 601}}$$

The value of  $\sigma_{ident,set}^{(m=8)}$  is given for the considered triplet on each graph of both Figure 7 and Figure 8.

Figure 7 a) corresponds to the triplet for which  $\sigma_{ident,set}^{(m=8)}$  is the highest among all 98 triplets for  $S(t) = 0$ . For this “worst” triplet, one has  $\sigma_{ident,set}^{(m=8)} = 0.070$  K. The “best” triplet, for which  $\sigma_{ident,set}^{(m=8)} = 0.001$  K, is not shown here. In Figure 7 a) and Figure 7 b), values of  $K$  are of the same magnitude. This is also the case for values of  $n$ . However, the flowrate  $Q_{in}$  is higher in Figure 7 b) than in Figure 7 a): increasing the flowrate induces larger viscous dissipation and hence larger temperature deviations.

Figure 7 b) shows temperature deviations reaching several tenths of K in steady state (about 90 K for temperature  $[\delta T_{obs}]_5$ ), which is not compatible with the assumption made in section 2.1.5 that the viscosity does not depend on temperature. Such temperature elevations occur for high values of  $K$ ,  $n$  and  $Q_{in}$  and a duration of several tenths of seconds. However, in practice, injection processes involving high flowrates last about 2 seconds only. During these first few seconds, the temperature elevation remains lower than 20 K, even for high values of  $K$  and  $n$  (see Figure 7 b)), and the non-dependence of viscosity with temperature can be assumed. Experiments lasting about 30 to 60 seconds may occur for material characterization when molds are taken apart, however in such cases the flowrate is quite low (10 to 20 cc.s<sup>-1</sup>) and the maximal temperature elevation is also about 20 K, even for high values of  $K$  and  $n$  (see Figure 7 a)). In fact, simulations of 60 seconds duration have been used in order to show the ability of the ROM to reproduce the FOM behavior in steady state, even if the non-dependence of viscosity with temperature is not always satisfied at long times.

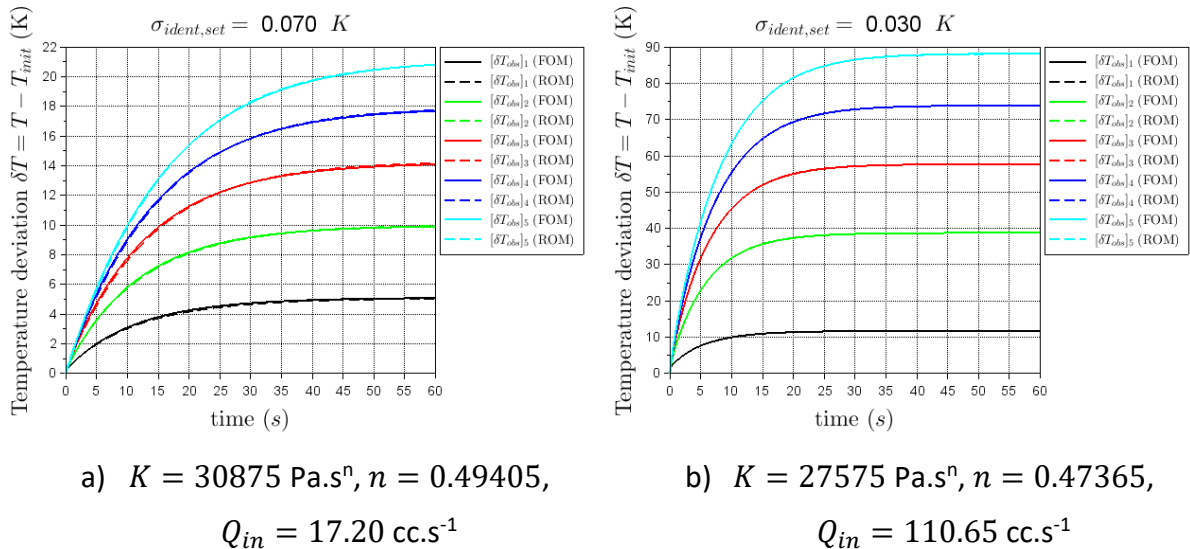
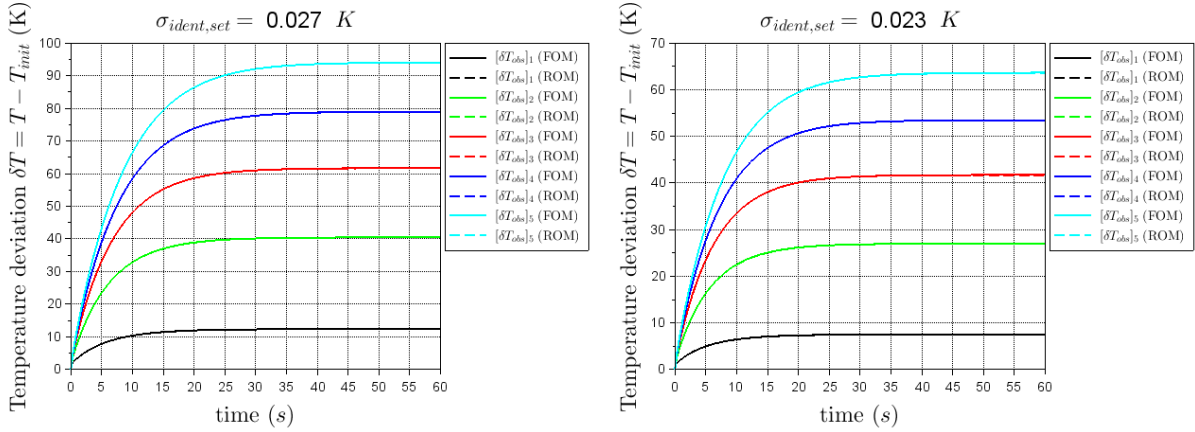


Figure 7. Identification: examples of temperature deviations computed by FOM and order 8 ROM for  $S(t) = 0 \text{ W}\cdot\text{m}^{-3}$

Figure 8 corresponds to the case  $S(t) = S^*(t)$  (step signal of magnitude  $8 \times 10^6 \text{ W}\cdot\text{m}^{-3}$ ). In Figure 8 a) and Figure 8 b), values of  $K$  are of the same magnitude. This is also the case for

values of  $Q_{in}$ . However,  $n$  is lower in Figure 8 b) than in Figure 8 a): according to Eq.(11) and Eq.(15), the viscous dissipation term is  $\varepsilon_v = K \dot{\gamma}^{n+1}$ , which decreases with  $n$ , thus inducing smaller temperature deviations. The triplet for which  $\sigma_{ident,set}^{(m=8)}$  is the highest among all 98 triplets for  $S(t) = S^*(t)$  is the same than for  $S(t) = 0$ . For this “worst” triplet, which is not shown here, one has  $\sigma_{ident,set}^{(m=8)} = 0.061$  K. The “best” triplet, for which  $\sigma_{ident,set}^{(m=8)} = 0.014$  K, is different from the “best” one for  $S(t) = 0$  and is also not shown here.



a)  $K = 34505 \text{ Pa}\cdot\text{s}^n, n = 0.44815,$

$Q_{in} = 100.75 \text{ cc}\cdot\text{s}^{-1}$

b)  $K = 32855 \text{ Pa}\cdot\text{s}^n, n = 0.36825,$

$Q_{in} = 111.75 \text{ cc}\cdot\text{s}^{-1}$

Figure 8. Identification: examples of temperature deviations computed by FOM and order 8 ROM for  $S(t) = S^*(t)$  (step signal  $8 \times 10^6 \text{ W}\cdot\text{m}^{-3}$ )

### 6.3 Validation of the identified ROMs

Some test cases have been conducted for the validation of the ROMs identified in the previous section 6.2. Computations were performed for 50 triplets  $(K, n, Q_{in})$  different of those used for the ROMs identification, however convergence was not obtained for one of them. The set of  $N_s^{val} = 49$  triplets  $(K, n, Q_{in})$  depicted by blue dots in Figure 5 has thus been used for validation purposes.

Two different validation tests have been performed:

- In test n°1, simulations using the identified ROMs have been performed for each one of the 49 triplets  $(K, n, Q_{in})$ , with the heat source signal  $S(t) = S^*(t)$  used for the identification, i.e. the step of magnitude  $8 \times 10^6 \text{ W}\cdot\text{m}^{-3}$  (we could also have used  $S(t) = 0$ ). This test allows to assess the robustness of the identified ROMs as regards to the viscosity parameters and inlet flowrate.
- In test n°2, simulations using the identified ROMs have been performed for each one of the 49 triplets  $(K, n, Q_{in})$ , with the test signal  $S^{test}(t)$  shown in Figure 9. This test

allows us to check the ability of the identified ROMs to work with heat source signals  $S(t)$  different than the step signal used for the identification.

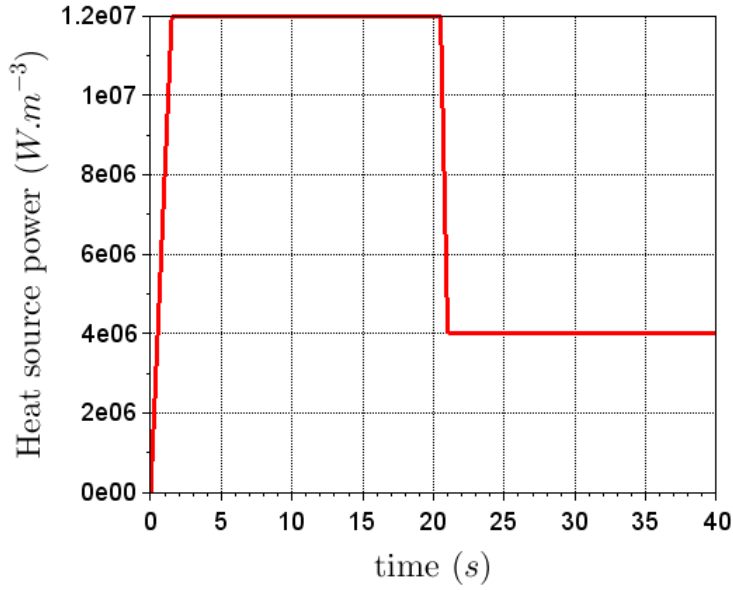


Figure 9. Heat source power test signal  $S^{test}(t)$

For each validation test, the 5 temperature evolutions  $\delta T_{obs}^{ROM}(t)$  are compared with those computed with the FOM for the same 49 triplets  $(K, n, Q_{in})$  and heat source signal. The time sampling is the same as for data used for ROMs identification. For each validation test, the mean quadratic global error  $\sigma_{valid}^{(m)}$  between FOM and ROM of order  $m$  as well as the mean quadratic error  $\sigma_{valid,set}^{(m)}(j), j \in \{1, \dots, 49\}$  associated to each test triplet  $(K, n, Q_{in})$ , are defined as follows:

$$\sigma_{valid}^{(m)} = \sqrt{\frac{\sum_{i=1}^{N_{obs}} \sum_{j=1}^{N_s^{val}} \sum_{k=1}^{N_t^{val}} \left( [\delta T_{obs}^{ROM}]_i(j, t_k) - [\delta T_{obs}^{FOM}]_i(j, t_k) \right)^2}{N_{obs} N_s^{val} N_t^{val}}}$$

$$\sigma_{valid,set}^{(m)}(j) = \sqrt{\frac{\sum_{i=1}^{N_{obs}} \sum_{k=1}^{N_t^{val}} \left( [\delta T_{obs}^{ROM}]_i(j, t_k) - [\delta T_{obs}^{FOM}]_i(j, t_k) \right)^2}{N_{obs} N_t^{val}}}, j \in \{1, \dots, N_s^{val}\}$$

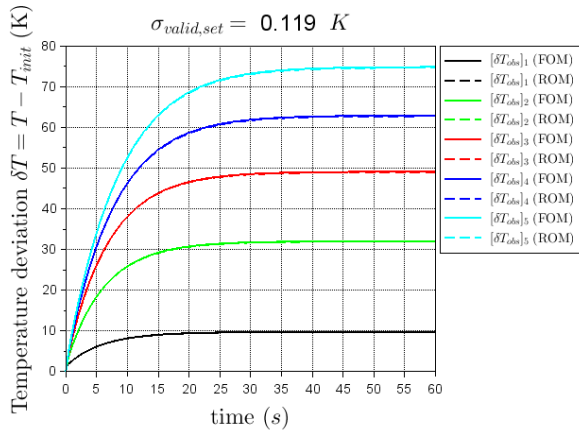
With  $N_t^{val} = 601$  for test n°1 and  $N_t^{val} = 401$  for test n°2 for which 40 s are simulated.

The value of  $\sigma_{valid}^{(m)}$  is shown in Figure 6 as a function of ROM order  $m$  for test n°1 (blue curve) and test n°2 (green curve). As for the identification phase,  $\sigma_{valid}^{(m)}$  decreases with the order  $m$ . However,  $\sigma_{valid}^{(m)}$  for test n°1 is very close to  $\sigma_{ident}^{(m)}$  for all values of  $m$ , thus showing the robustness of the ROMs as regards to the  $(K, n, Q_{in})$  values, whereas  $\sigma_{valid}^{(m)}$  for test n°2 is slightly less close to  $\sigma_{ident}^{(m)}$ . This is due to the fact that for test n°2, the heat source signal  $S^{test}(t)$  is also different from the one used for the ROMs identification. Nevertheless, for ROM

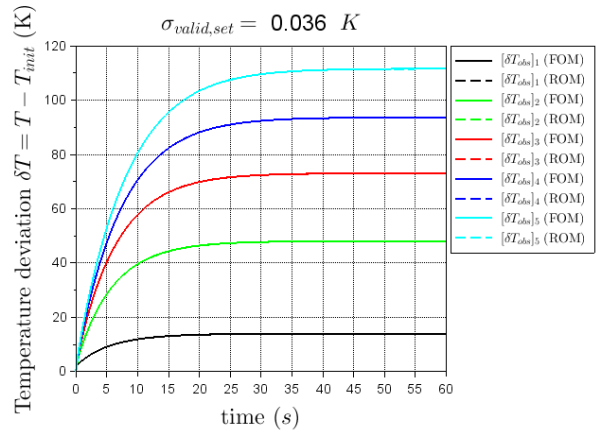
of order 8, the values of  $\sigma_{valid}^{(m=8)}$  for both tests almost reach the value of  $\sigma_{ident}^{(m=8)}$ :  $\sigma_{valid}^{(m=8)} = 0.037$  K for test n°1 and  $\sigma_{valid}^{(m=8)} = 0.051$  K for test n°2, showing the robustness of the ROMs whatever the value of the inputs parameters ( $K, n, Q_{in}$ ) and the applied heat source signal.

In addition, some examples of evolutions of temperature deviations for 4 different triplets ( $K, n, Q_{in}$ ) are shown in Figure 10 for test n°1 and in Figure 11 for test n°2. The graphs a) to d) in both figures assess the ability of the identified order 8 ROM to reproduce the FOM outputs. Once again, dynamics and temperature magnitude are different depending on the triplet ( $K, n, Q_{in}$ ).

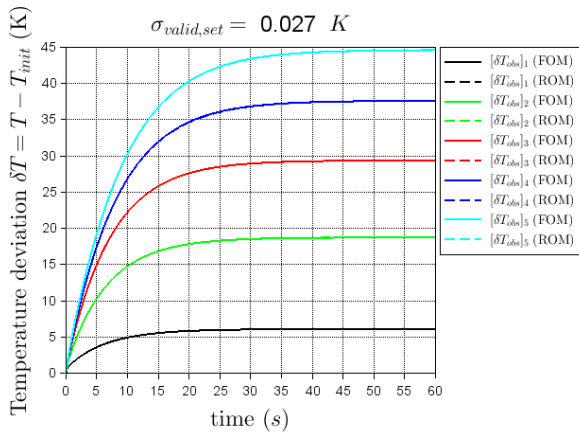
Figure 10 a) corresponds to the triplet for which  $\sigma_{valid,set}^{(m=8)}$  is the highest among all 49 triplets for  $S(t) = S^*(t)$ . For this “worst” triplet, one has  $\sigma_{valid,set}^{(m=8)} = 0.119$  K. In Figure 10 a), Figure 10 b) and Figure 10 d), values of  $n$  are of the same magnitude. This is also the case for values of  $Q_{in}$ . However,  $K$  is higher in Figure 10 b) than in Figure 10 a): increasing the flowrate induces larger viscous dissipation and hence larger temperature deviations. Figure 10 d) and Figure 10 a) show that a lower value of  $K$  leads to lower temperatures deviations.



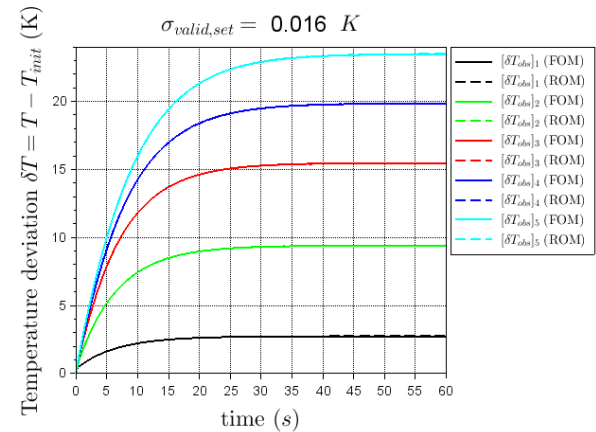
a)  $K = 24110$  Pa.s<sup>n</sup>,  $n = 0.4677$ ,  
 $Q_{in} = 101.00$  cc.s<sup>-1</sup>



b)  $K = 34670$  Pa.s<sup>n</sup>,  $n = 0.4609$ ,  
 $Q_{in} = 114.50$  cc.s<sup>-1</sup>



c)  $K = 32690$  Pa.s<sup>n</sup>,  $n = 0.3521$ ,



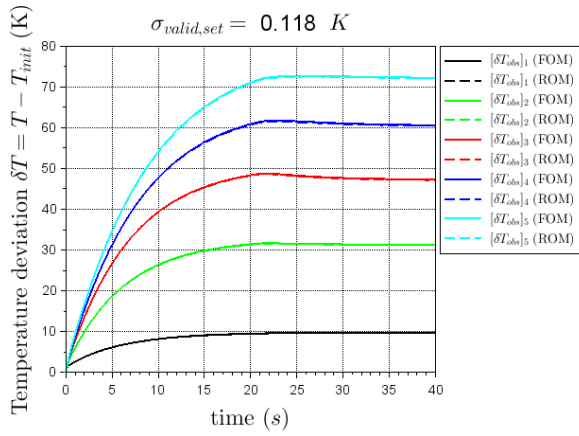
d)  $K = 6290$  Pa.s<sup>n</sup>,  $n = 0.4745$ ,

$$Q_{in} = 72.70 \text{ cc.s}^{-1}$$

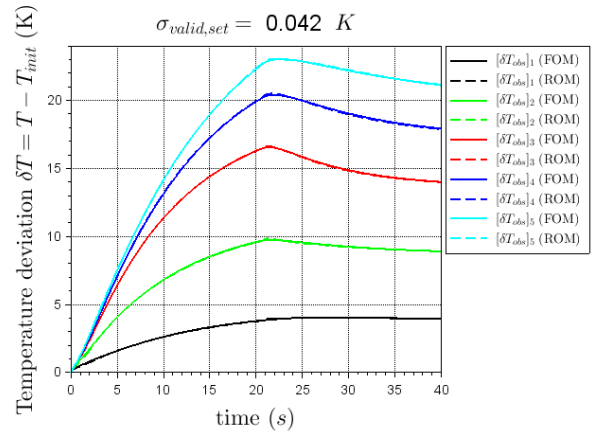
$$Q_{in} = 94.7 \text{ cc.s}^{-1}$$

Figure 10. Validation: examples of temperature deviations computed by FOM and order 8 ROM for test n°1 for which  $S(t) = S^*(t)$  (step signal  $8 \times 10^6 \text{ W.m}^{-3}$ )

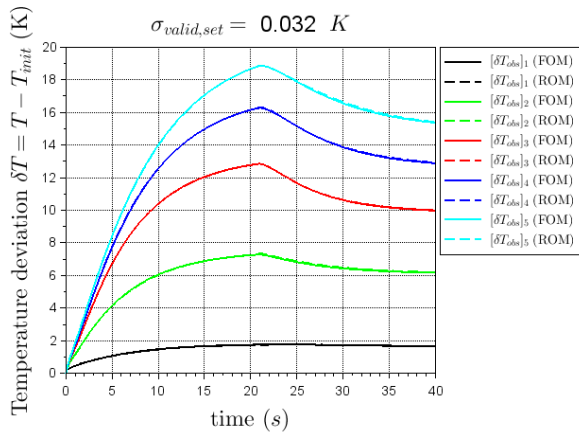
Figure 11 a) corresponds to the triplet for which  $\sigma_{valid,set}^{(m=8)}$  is the highest among all 49 triplets for  $S(t) = S^{test}(t)$ . For this “worst” triplet, which is the same than in test n°1, one has  $\sigma_{valid,set}^{(m=8)} = 0.118 \text{ K}$ . For high values of  $K$ ,  $n$  and  $Q_{in}$ , the viscous dissipation is large and its effects on the temperature dynamics are preponderant compared to those of the applied heat source  $S^{test}(t)$  which are hardly visible (cf. Figure 11 a)). For high values of  $K$  but low values of  $n$  and  $Q_{in}$  (Figure 11 b)) and high values of  $Q_{in}$  but low values of  $K$  and  $n$  (Figure 11 c)), the viscous dissipation is lower and the effects of the applied heat source are more noticeable. For low values of  $K$ ,  $n$  and  $Q_{in}$ , the viscous dissipation is low and the effects of the applied heat source  $S^{test}(t)$  are preponderant (cf. Figure 11 d)).



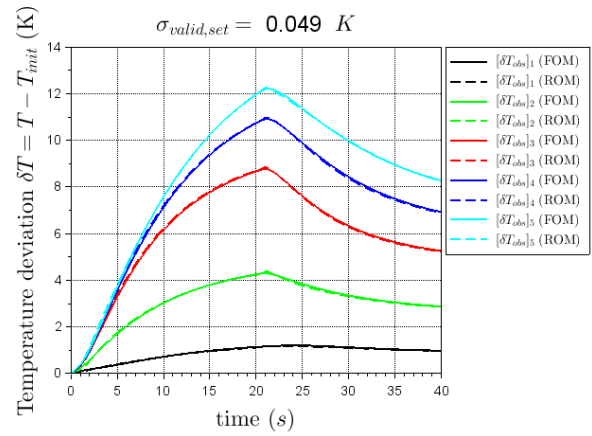
a)  $K = 24110 \text{ Pa.s}^n$ ,  $n = 0.4677$ ,  
 $Q_{in} = 101.00 \text{ cc.s}^{-1}$



b)  $K = 31370 \text{ Pa.s}^n$ ,  $n = 0.3623$ ,  
 $Q_{in} = 22.10 \text{ cc.s}^{-1}$



c)  $K = 7610 \text{ Pa.s}^n$ ,  $n = 0.3589$ ,  
 $Q_{in} = 106.00 \text{ cc.s}^{-1}$



d)  $K = 4310 \text{ Pa.s}^n$ ,  $n = 0.3759$ ,  
 $Q_{in} = 35.3 \text{ cc.s}^{-1}$

Figure 11. Validation: examples of temperature deviations computed by FOM and order 8 ROM for test n°2 for which  $S(t) = S^{test}(t)$

## 6.4 Computing time

### 6.4.1 ROMs construction

The construction of ROMs using the MIM requires some time, which depends on the number of outputs  $N_{obs}$ , the number of data triplets  $N_s^{id}$ , the number of time instants  $N_t^{id}$  and the number of iterations performed. In Table 1 are shown the computing times for building ROMs of order 1 to 8 in the present case. Although the ROMs identification procedure takes some time, this is done offline and once ROMs are built, each execution requires only a very short computing time so that ROMs can be used online, as shown in the next section.

ROM order $m$	1	2	3	4	5	6	7	8
Number of iterations	4000	6000	8000	10,000	12,000	15,000	18,000	21,000
Computing time (CPU s)	355	686	1259	1941	2897	4426	8985	12,355

Table 1. Computing time for ROMs construction

### 6.4.2 ROMs execution versus ANSYS® POLYFLOW® FOM

With the ANSYS® POLYFLOW® FOM using a variable time step (from 0.001 s to about 0.1 s), the computing time for a single simulation of 60 s duration is about 8500 s (depending on values of  $K$ ,  $n$  and  $Q_{in}$  and on the applied heat source) on a personal computer (i5-8400H@2.5GHz, 16Go RAM). The ROMs allow using constant time step (0.1 s). The computing time ranges from 0.24 s for the order 1 ROM to 0.41 s for the order 8 ROM. The order 8 ROM thus allows a gain factor of about  $2 \times 10^4$  compared to the ANSYS® POLYFLOW® FOM.

## 7 Conclusion

In the frame of melted polymer flows characterization, incompressible flows of non-Newtonian fluids, more precisely generalized Newtonian fluids, have been considered. The problem is assumed as quasi-static for the fluid flow and unsteady for the thermal state. The construction of thermo-rheological Reduced Order Models (ROMs) by the Modal Identification Method (MIM), has been presented and performed. The formulation of nonlinear ROMs has been developed in order to obtain an explicit parametrization by consistency index  $K$  and pseudoplastic index  $n$  characterizing the power-law viscosity model, as well as inlet flowrate  $Q_{in}$ . An original approach has allowed handling the issues involved by the pseudoplastic index  $n$  acting as an exponent in the power-law viscosity model. Several possible time-varying boundary conditions and source terms also appear in the ROMs

formulation. ROMs have been built by minimizing a quadratic functional based on the difference between the outputs (computed temperatures at chosen locations of interest) of a reference Full Order Model (FOM) and those of the ROMs, for the same inputs, here a set of triplets  $(K, n, Q_{in})$  and an applied time-varying volumetric heat source power. The developed approach has been applied to a laminar polymer flow in an annular duct, corresponding to an experimental set-up which will be used for process control purposes. The reference FOM is a two-dimensional axisymmetric ANSYS® POLYFLOW® Finite Elements model. First, a series of ROMs of order 1 to 8 has been built, using as data temperature deviations corresponding to a set of triplets  $(K, n, Q_{in})$ , with and without extra heat source applied. The temperature evolutions exhibit various dynamics, depending on the input parameters. Once identified, the ROMs have been tested with another set of triplets  $(K, n, Q_{in})$  and two heat source power signals, the first one being the signal used for the ROMs construction, the second one being different. These tests have shown the capability of the ROMs, especially the ROM of order 8, to reproduce the temperature deviations computed with the reference FOM. Parameters  $K$ ,  $n$  and  $Q_{in}$  appear explicitly in the ROMs, allowing to use them for parametric studies or for the estimation of  $K$  and  $n$  from temperature measurements through an inverse problem, provided that sensitivities of temperatures with respect to these parameters are large enough. Because of their very low computing times compared to the reference FOM, ROMs can be used for in-line estimation of  $K$  and  $n$  from temperature measurements on the central axis. A ROM has actually been used in the inverse problem for estimating the parameters of the power-law model for a real polymer, from temperature measurements recorded on the experimental set-up. The temperatures computed by the ROM with the estimated power-law parameters fit the experimental data, and the power-law viscosity is in accordance with the Cross model on a large shear rate range, except for very low and very high shear rate values, of course. These results are out of the scope of the present paper and will be presented in a future publication.

## Appendix

### A.1 Galerkin projections of local equations

#### A.1.1 Momentum conservation equation

Let us introduce the residue  $\overline{\mathcal{R}_v}(\bar{x})$  of momentum equation (17). The Galerkin projection consists in forcing  $\overline{\mathcal{R}_v}(\bar{x})$ , written with approximations of variables, to be orthogonal to each  $\bar{\phi}_k^v(\bar{x})$ ,  $k \in \{1, \dots, m_v\}$ , so that the projection of the residue onto the subspace of  $[\mathcal{L}_2(\Omega_f)]^d$  generated by the  $\bar{\phi}_k^v$  is null. According to the inner product (31), it writes:

$$\langle \overline{\mathcal{R}_v}(\bar{x}), \bar{\phi}_k^v(\bar{x}) \rangle_{\Omega_f} = \int_{\Omega_f} \overline{\mathcal{R}_v}(\bar{x}, t) \cdot \bar{\phi}_k^v(\bar{x}) d\Omega = 0 \quad \forall k \in \{1, \dots, m_v\} \quad (\text{A.1})$$

According to (17), equation (A.1) writes:

$$\underbrace{\int_{\Omega_f} \overline{\text{grad} p} \cdot \bar{\phi}_k^v d\Omega}_{\mathcal{P}_v} - \underbrace{\int_{\Omega_f} \overline{\text{div}} \left( \eta \left( \overline{\text{grad}}(\bar{v}) + \left( \overline{\text{grad}}(\bar{v}) \right)^T \right) \right) \cdot \bar{\phi}_k^v d\Omega}_{\mathcal{D}_v} = 0 \quad (\text{A.2})$$

$\forall k \in \{1, \dots, m_v\}$

The following steps, not detailed here, are then performed on equation (A.2):

- The pressure term  $\mathcal{P}_v$  is integrated by parts using  $\int_{\Omega_f} f \text{div}(\bar{u}) d\Omega = \int_{\Gamma_f} f \bar{u} \cdot \bar{n} d\Gamma - \int_{\Omega_f} \bar{u} \cdot \overline{\text{grad}} f d\Omega$ . The resulting term on  $\Omega_f$  is null due to equation (32);
- The viscous diffusion term  $\mathcal{D}_v$  is integrated by parts using  $\int_{\Omega_f} \overline{\text{div}}(\bar{M}) \cdot \bar{u} d\Omega = \int_{\Gamma_f} (\bar{u} \cdot \bar{M}) \cdot \bar{n} d\Gamma - \int_{\Omega_f} \bar{M}^T : \overline{\text{grad}}(\bar{u}) d\Omega$ . The symmetry of tensor  $\eta \left( \overline{\text{grad}}(\bar{v}) + \left( \overline{\text{grad}}(\bar{v}) \right)^T \right)$  is taken into account in the resulting term on  $\Omega_f$ . The resulting term on  $\Gamma_f$  is split into two terms. In the term  $-\int_{\Gamma_f} \left( \bar{\phi}_k^v \cdot \left( \eta \overline{\text{grad}}(\bar{v}) \right) \right) \cdot \bar{n} d\Gamma$ , using  $(\bar{a} \cdot \bar{M}) \cdot \bar{b} = \bar{a} \cdot (\bar{M} \cdot \bar{b})$  allows to introduce boundary condition (22) and using  $\overline{\text{grad}}(\bar{a} \cdot \bar{b}) = \bar{a} \cdot \overline{\text{grad}} \bar{b} + \bar{b} \cdot \overline{\text{grad}} \bar{a}$  allows to introduce boundary conditions (20) and (26);
- Approximations (30) for  $\bar{v}(\bar{x})$ , (33) for  $p(\bar{x})$  and (35) for  $\eta(\bar{x})$ , are injected in the remaining internal and boundary terms.

Equation (A.2) is finally written as:

$$\sum_{i=1}^{m_p} [M_{vp}]_{ki} a_i^p + \sum_{i=1}^{m_\eta} \sum_{j=1}^{m_v} [E_v]_{kij} a_i^\eta a_j^v + Q_{in} \sum_{i=1}^{m_\eta} [M_{v\eta}]_{ki} a_i^\eta = 0 \quad \forall k \in \{1, \dots, m_v\} \quad (\text{A.3})$$

Where:

$$[M_{vp}]_{ki} = \int_{\Gamma_f} \phi_i^p \bar{\phi}_k^v \cdot \bar{n} d\Gamma \quad \forall k \in \{1, \dots, m_v\}, \forall i \in \{1, \dots, m_p\}$$

$$[E_v]_{kij} = \int_{\Omega_f} \left( \phi_i^\eta \left( \overline{\text{grad}}(\bar{\phi}_j^v) + \left( \overline{\text{grad}}(\bar{\phi}_j^v) \right)^T \right) \right) : \overline{\text{grad}}(\bar{\phi}_k^v) d\Omega$$

$$- \int_{\Gamma_{in} \cup \Gamma_{sf}} \phi_i^\eta \overline{\text{grad}}(\bar{\phi}_j^v \cdot \bar{\phi}_k^v) \cdot \bar{n} d\Gamma - \int_{\Gamma_f} \left( \bar{\phi}_k^v \cdot \left( \phi_i^\eta \left( \overline{\text{grad}}(\bar{\phi}_j^v) \right)^T \right) \right) \cdot \bar{n} d\Gamma$$

$\forall k \in \{1, \dots, m_v\}, \forall i \in \{1, \dots, m_\eta\}, \forall j \in \{1, \dots, m_v\}$

$$[M_{v\eta}]_{ki} = - \int_{\Gamma_{in}} \phi_i^\eta F_{v_{in}} \bar{n} \cdot \left( \overline{\text{grad}}(\bar{\phi}_k^v) \cdot \bar{n} \right) d\Gamma \quad \forall k \in \{1, \dots, m_v\}, \forall i \in \{1, \dots, m_\eta\} \quad (\text{A.4})$$

## A.1.2 Poisson equation for pressure

Calling  $\mathcal{R}_p(\bar{x})$  the residue of Poisson equation (19), the Galerkin projection using the inner product (36) writes:

$$\langle \mathcal{R}_p, \phi_k^p \rangle_{\Omega_f} = \int_{\Omega_f} \mathcal{R}_p \phi_k^p d\Omega = 0 \quad \forall k \in \{1, \dots, m_p\} \quad (\text{A.5})$$

According to (19), equation (A.5) writes:

$$\underbrace{\int_{\Omega_f} \text{div}(\overline{\text{grad}}p) \phi_k^p d\Omega}_{\mathcal{A}_p} - \underbrace{\int_{\Omega_f} \text{div} \left( \overline{\text{div}} \left( \eta \left( \overline{\text{grad}}(\bar{v}) + \left( \overline{\text{grad}}(\bar{v}) \right)^T \right) \right) \right)}_{\mathcal{B}_p} \phi_k^p d\Omega = 0 \quad \forall k \in \{1, \dots, m_p\} \quad (\text{A.6})$$

Using approximations (30) for  $\bar{v}(\bar{x})$ , (33) for  $p(\bar{x})$  and (35) for  $\eta(\bar{x})$ , equation (A.6) writes:

$$\sum_{i=1}^{m_p} [M_p]_{ki} a_i^p = \sum_{i=1}^{m_\eta} \sum_{j=1}^{m_v} [E_p]_{kij} a_i^\eta a_j^v \quad \forall k \in \{1, \dots, m_p\} \quad (\text{A.7})$$

Where:

$$[M_p]_{ki} = \int_{\Omega_f} \text{div}(\overline{\text{grad}}\phi_i^p) \phi_k^p d\Omega \quad \forall k \in \{1, \dots, m_p\}, \forall i \in \{1, \dots, m_p\} \quad (\text{A.8})$$

$$[E_p]_{kij} = \int_{\Omega_f} \text{div} \left( \overline{\text{div}} \left( \phi_i^\eta \left( \overline{\text{grad}}(\bar{\phi}_j^v) + \left( \overline{\text{grad}}(\bar{\phi}_j^v) \right)^T \right) \right) \right) \phi_k^p d\Omega$$

$$\forall k \in \{1, \dots, m_p\}, \forall i \in \{1, \dots, m_\eta\}, \forall j \in \{1, \dots, m_v\}$$

It would have been possible to perform an integration by parts of  $\mathcal{A}_p$  in equation (A.6) in order to introduce Neumann boundary conditions for pressure. However, these boundary conditions are usually either homogeneous or expressed through a projection of the momentum equation on the local outward unit vector normal to the boundary. Hence an equation similar to (A.7) would have been obtained.

### A.1.3 Equation defining function $g$

Calling  $\mathcal{R}_g(\bar{x})$  the residue of equation (13), the Galerkin projection using the inner product (36) writes:

$$\langle \mathcal{R}_g, \phi_k^g \rangle_{\Omega_f} = \int_{\Omega_f} \mathcal{R}_g \phi_k^g d\Omega = 0 \quad \forall k \in \{1, \dots, m_g\} \quad (\text{A.9})$$

According to (13), equation (A.9) writes:

$$\underbrace{\int_{\Omega_f} g \phi_k^g d\Omega}_{\mathcal{A}_g} - \underbrace{\int_{\Omega_f} \frac{1}{2} \left( \overline{\text{grad}}(\bar{v}) + \left( \overline{\text{grad}}(\bar{v}) \right)^T \right) : \left( \overline{\text{grad}}(\bar{v}) + \left( \overline{\text{grad}}(\bar{v}) \right)^T \right)}_{\mathcal{B}_g} \phi_k^g d\Omega = 0 \quad \forall k \in \{1, \dots, m_g\} \quad (\text{A.10})$$

Using approximations (30) for  $\bar{v}(\bar{x})$  and (34) for  $g(\bar{x})$  and taking into account (37) in the term  $\mathcal{A}_g$ , equation (A.10) writes:

$$a_k^g = \sum_{i=1}^{m_v} \sum_{j=1}^{m_v} [E_g]_{kij} a_i^v a_j^v \quad \forall k \in \{1, \dots, m_g\} \quad (\text{A.11})$$

Where:

$$[E_g]_{kij} = \frac{1}{2} \int_{\Omega_f} \left( \overline{\text{grad}} \bar{\phi}_i^v + (\overline{\text{grad}} \bar{\phi}_i^v)^T \right) : \left( \overline{\text{grad}} \bar{\phi}_j^v + (\overline{\text{grad}} \bar{\phi}_j^v)^T \right) \phi_k^g d\Omega$$

$$\forall k \in \{1, \dots, m_g\}, \forall i \in \{1, \dots, m_v\}, \forall j \in \{1, \dots, m_v\}$$

#### A.1.4 Dynamic viscosity power-law model

The pseudoplastic index  $n$  acting as an exponent in the power-law model (16) would lead to the term  $\int_{\Omega_f} \left( \sum_{i=1}^{m_g} \phi_i^g(\bar{x}) a_i^g \right)^{\frac{n-1}{2}} \phi_k^\eta d\Omega$  in the Galerkin projection of Eq.(16). The impossibility to “take  $n$  out” of the integral would thus be an issue. Using logarithms will lead to another issue that can nevertheless be overcome. Taking the logarithm of Eq.(16), we get:

$$\ln(\eta) = \ln(K) + \left( \frac{n-1}{2} \right) \ln(g) \quad (\text{A.12})$$

Calling  $\mathcal{R}_\eta(\bar{x})$  the residue of equation (A.12), the Galerkin projection using the inner product (36) writes:

$$\langle \mathcal{R}_\eta, \phi_k^\eta \rangle_{\Omega_f} = \int_{\Omega_f} \mathcal{R}_\eta \phi_k^\eta d\Omega = 0 \quad \forall k \in \{1, \dots, m_\eta\} \quad (\text{A.13})$$

According to (A.12), equation (A.13) writes:

$$\int_{\Omega_f} \ln(\eta) \phi_k^\eta d\Omega - \ln(K) \int_{\Omega_f} \phi_k^\eta d\Omega - \left( \frac{n-1}{2} \right) \int_{\Omega_f} \ln(g) \phi_k^\eta d\Omega = 0 \quad \forall k \in \{1, \dots, m_\eta\} \quad (\text{A.14})$$

Using approximations (35) for  $\eta(\bar{x})$  and (34) for  $g(\bar{x})$ , one obtains terms  $\ln(\sum_{i=1}^{m_\eta} \phi_i^\eta(\bar{x}) a_i^\eta)$  and  $\ln(\sum_{i=1}^{m_g} \phi_i^g(\bar{x}) a_i^g)$ . In order to deal with these terms of the form  $\ln(\sum \dots)$ , they are written as:

$$\ln \left( \phi_1^\eta(\bar{x}) a_1^\eta \left( 1 + \sum_{i=2}^{m_\eta} \frac{\phi_i^\eta(\bar{x}) a_i^\eta}{\phi_1^\eta(\bar{x}) a_1^\eta} \right) \right) \text{ and } \ln \left( \phi_1^g(\bar{x}) a_1^g \left( 1 + \sum_{i=2}^{m_g} \frac{\phi_i^g(\bar{x}) a_i^g}{\phi_1^g(\bar{x}) a_1^g} \right) \right)$$

And then:

$$\ln(\phi_1^\eta(\bar{x}) a_1^\eta) + \ln \left( 1 + \sum_{i=2}^{m_\eta} \frac{\phi_i^\eta(\bar{x}) a_i^\eta}{\phi_1^\eta(\bar{x}) a_1^\eta} \right) \text{ and } \ln(\phi_1^g(\bar{x}) a_1^g) + \ln \left( 1 + \sum_{i=2}^{m_g} \frac{\phi_i^g(\bar{x}) a_i^g}{\phi_1^g(\bar{x}) a_1^g} \right)$$

In order to handle the terms of the form  $\ln(1 + \sum \dots)$ , we make the hypothesis, verified in practice in the MIM, that first terms  $\phi_1^\eta(\bar{x}) a_1^\eta$  and  $\phi_1^g(\bar{x}) a_1^g$  in respective approximations (35) and (34) are preponderant compared to the higher order terms:

$$\begin{aligned}\phi_1^\eta(\bar{x})a_1^\eta &\gg \sum_{i=2}^{m_\eta} \phi_i^\eta(\bar{x})a_i^\eta \Rightarrow \sum_{i=2}^{m_\eta} \frac{\phi_i^\eta(\bar{x})a_i^\eta}{\phi_1^\eta(\bar{x})a_1^\eta} \ll 1 \\ \phi_1^g(\bar{x})a_1^g &\gg \sum_{i=2}^{m_g} \phi_i^g(\bar{x})a_i^g \Rightarrow \sum_{i=2}^{m_g} \frac{\phi_i^g(\bar{x})a_i^g}{\phi_1^g(\bar{x})a_1^g} \ll 1\end{aligned}$$

We can thus use the Taylor series of  $\ln(1+x)$  around  $x=0$ :

$$\ln(1+x) = x - \frac{x^2}{2} + \frac{x^3}{3} + \dots + (-1)^{n-1} \frac{x^n}{n} + o(x^n) \quad (\text{A.15})$$

Using (A.15) at first order for terms of the form  $\ln(1+\sum \dots)$ , equation (A.14) writes:

$$\begin{aligned}\int_{\Omega_f} \left( \ln(\phi_1^\eta(\bar{x})) + \ln(a_1^\eta) + \sum_{i=2}^{m_\eta} \frac{\phi_i^\eta(\bar{x})a_i^\eta}{\phi_1^\eta(\bar{x})a_1^\eta} \right) \phi_k^\eta(\bar{x}) d\Omega - \ln(K) \int_{\Omega_f} \phi_k^\eta(\bar{x}) d\Omega \\ - \left( \frac{n-1}{2} \right) \int_{\Omega_f} \left( \ln(\phi_1^g(\bar{x})) + \ln(a_1^g) + \sum_{i=2}^{m_g} \frac{\phi_i^g(\bar{x})a_i^g}{\phi_1^g(\bar{x})a_1^g} \right) \phi_k^\eta(\bar{x}) d\Omega \\ = 0 \quad \forall k \in \{1, \dots, m_\eta\}\end{aligned} \quad (\text{A.16})$$

Vectors  $b^\eta \in \mathbb{R}^m$  and  $b^g \in \mathbb{R}^m$  are now defined as:

$$b_1^\eta = \ln(a_1^\eta); \quad b_i^\eta = \frac{a_i^\eta}{a_1^\eta} \quad \forall i \in \{2, \dots, m_\eta\} \quad (\text{A.17})$$

$$b_1^g = \ln(a_1^g); \quad b_i^g = \frac{a_i^g}{a_1^g} \quad \forall i \in \{2, \dots, m_g\} \quad (\text{A.18})$$

The following matrices and vectors are also defined:

$$[M_{\eta\eta}]_{ki} = \int_{\Omega_f} \frac{\phi_i^\eta(\bar{x})}{\phi_1^\eta(\bar{x})} \phi_k^\eta(\bar{x}) d\Omega \quad \forall k \in \{1, \dots, m_\eta\}, \forall i \in \{1, \dots, m_\eta\} \quad (\text{A.19})$$

$$[M_{\eta g}]_{ki} = \int_{\Omega_f} \frac{\phi_i^g(\bar{x})}{\phi_1^g(\bar{x})} \phi_k^\eta(\bar{x}) d\Omega \quad \forall k \in \{1, \dots, m_\eta\}, \forall i \in \{1, \dots, m_g\} \quad (\text{A.20})$$

$$[U_\eta]_k = [M_{\eta\eta}]_{k1} = [M_{\eta g}]_{k1} = \int_{\Omega_f} \phi_k^\eta(\bar{x}) d\Omega \quad \forall k \in \{1, \dots, m_\eta\} \quad (\text{A.21})$$

$$[W_{\eta\eta}]_k = - \int_{\Omega_f} \ln(\phi_1^\eta(\bar{x})) \phi_k^\eta(\bar{x}) d\Omega \quad \forall k \in \{1, \dots, m_\eta\}$$

$$[W_{\eta g}]_k = \int_{\Omega_f} \ln(\phi_1^g(\bar{x})) \phi_k^\eta(\bar{x}) d\Omega \quad \forall k \in \{1, \dots, m_\eta\}$$

Taking into account (A.17) to (A.21) and the two above equations, equation (A.16) writes:

$$\sum_{i=1}^{m_\eta} [M_{\eta\eta}]_{ki} b_i^\eta = [W_{\eta\eta}]_k + \ln(K) [U_\eta]_k + \left( \frac{n-1}{2} \right) \left( [W_{\eta g}]_k + \sum_{i=1}^{m_g} [M_{\eta g}]_{ki} b_i^g \right) \quad (\text{A.22})$$

$$\forall k \in \{1, \dots, m_\eta\}$$

### A.1.5 Energy conservation equation

Calling  $\mathcal{R}_e(\bar{x}, t)$  the residue of equation (18), the Galerkin projection using the weighted inner product (28) writes:

$$\langle \mathcal{R}_e, \phi_k^T \rangle_{\rho C_p} = \int_{\Omega} \rho C_p \mathcal{R}_e \phi_k^T d\Omega = 0 \quad \forall k \in \{1, \dots, m_T\} \quad (\text{A.23})$$

According to (18) and taking into account that transport and viscous dissipation terms are restricted to the fluid domain  $\Omega_f$  as  $\bar{v} = \bar{0}$  et  $g = 0$  in the solid domain  $\Omega_s$ , equation (A.23) writes:

$$\begin{aligned} \langle \mathcal{R}_e, \phi_k^T \rangle_{\rho C_p} &= \underbrace{\int_{\Omega} \rho C_p \frac{\partial T}{\partial t} \phi_k^T d\Omega}_{\mathcal{I}_e} + \underbrace{\int_{\Omega_f} \rho C_p \text{div}(T\bar{v}) \phi_k^T d\Omega}_{\mathcal{T}_e} - \underbrace{\int_{\Omega} \text{div}(\lambda \overline{\text{grad}} T) \phi_k^T d\Omega}_{\mathcal{D}_e} \\ &\quad - \underbrace{\int_{\Omega} \chi_S S(t) \phi_k^T d\Omega}_{\mathcal{S}_e} - \underbrace{\int_{\Omega_f} \eta g \phi_k^T d\Omega}_{\mathcal{V}_e} = 0 \quad \forall k \in \{1, \dots, m_T\} \end{aligned} \quad (\text{A.24})$$

The following steps, not detailed here, are then performed on equation (A.24):

- The transport term  $\mathcal{T}_e$  is integrated by parts using  $\int_{\Omega_f} f \text{div}(\bar{u}) d\Omega = \int_{\Gamma_f} f \bar{u} \cdot \bar{n} d\Gamma - \int_{\Omega_f} \bar{u} \cdot \overline{\text{grad}} f d\Omega$ , allowing to introduce boundary conditions (20), (21) and (26);
- The diffusion term  $\mathcal{D}_e$  is integrated by parts using  $\int_{\Omega} f \text{div}(\bar{u}) d\Omega = \int_{\Gamma} f \bar{u} \cdot \bar{n} d\Gamma - \int_{\Omega} \bar{u} \cdot \overline{\text{grad}} f d\Omega$ , allowing to introduce boundary conditions (23) and (24). Then, using  $\overline{\text{grad}}(f_1 f_2) = f_1 \overline{\text{grad}} f_2 + f_2 \overline{\text{grad}} f_1$  allows to introduce boundary conditions (21) and (25);
- Approximations (27) for  $T(\bar{x}, t)$ , (30) for  $\bar{v}(\bar{x})$ , (35) for  $\eta(\bar{x})$  and (34) for  $g(\bar{x})$ , are injected in the remaining internal and boundary terms, taking into account (29) in the term  $\mathcal{I}_e$ .

Equation (A.24) is finally written as:

$$\begin{aligned} \frac{da_k^T(t)}{dt} &= \sum_{i=1}^{m_T} [M_T]_{ki} a_i^T(t) + \sum_{i=1}^{m_v} \sum_{j=1}^{m_T} [E_{tr}]_{kij} a_i^v a_j^T(t) + \sum_{i=1}^{m_\eta} \sum_{j=1}^{m_g} [E_{dv}]_{kij} a_i^\eta a_j^g \\ &\quad + [V_S]_k S(t) + [V_{int}]_k Q_{in} T_{in}(t) + [V_\varphi]_k \varphi(t) + [V_{ind}]_k T_{in}(t) + [V_w]_k T_w(t) \\ &\quad \forall k \in \{1, \dots, m_T\} \end{aligned} \quad (\text{A.25})$$

Where:

$$\begin{aligned} [E_{tr}]_{kij} &= \int_{\Omega_f} \phi_j^T \bar{\phi}_i^v \cdot \overline{\text{grad}}(\rho C_p \phi_k^T) d\Omega - \int_{\Gamma_{out}} \rho C_p \phi_k^T \phi_j^T \bar{\phi}_i^v \cdot \bar{n} d\Gamma \\ &\quad \forall k \in \{1, \dots, m_T\}, \forall i \in \{1, \dots, m_v\}, \forall j \in \{1, \dots, m_T\} \end{aligned}$$

$$\begin{aligned}
[E_{dv}]_{kij} &= \int_{\Omega_f} \phi_i^\eta \phi_j^g \phi_k^T d\Omega \quad \forall k \in \{1, \dots, m_T\}, \forall i \in \{1, \dots, m_\eta\}, \forall j \in \{1, \dots, m_g\} \\
[M_T]_{ki} &= - \int_{\Omega} \lambda \overline{\text{grad}} \phi_i^T \cdot \overline{\text{grad}} \phi_k^T d\Omega + \int_{\Gamma_{in} \cup \Gamma_d} \lambda \overline{\text{grad}}(\phi_k^T \phi_i^T) \cdot \bar{n} d\Gamma \\
&\quad \forall k \in \{1, \dots, m_T\}, \forall i \in \{1, \dots, m_T\}
\end{aligned} \tag{A.26}$$

And  $\forall k \in \{1, \dots, m_T\}$ :  $[V_S]_k = \int_{\Omega} \chi_S \phi_k^T d\Omega$ ,  $[V_{int}]_k = \int_{\Gamma_{in}} \rho C_p F_{v_{in}} F_{T_{in}} \phi_k^T d\Gamma$ ,  
 $[V_\varphi]_k = \int_{\Gamma_n} \phi_k^T F_\varphi d\Gamma$ ,  $[V_{ind}]_k = - \int_{\Gamma_{in}} \lambda F_{T_{in}} \overline{\text{grad}} \phi_k^T \cdot \bar{n} d\Gamma$ ,  $[V_w]_k = - \int_{\Gamma_d} \lambda F_{T_w} \overline{\text{grad}} \phi_k^T \cdot \bar{n} d\Gamma$

## A.2 Proof that matrices $M_p$ and $M_{\eta\eta}$ are invertible

It can be shown that according to the fact that space functions  $\phi_i^p(\bar{x})$ ,  $i \in \{1, \dots, m_p\}$  and  $\phi_i^\eta(\bar{x})$ ,  $i \in \{1, \dots, m_\eta\}$  are truncations of bases (see section 4.1), matrices  $M_p$  defined by (A.8) and  $M_{\eta\eta}$  defined by (A.19) are invertible. In practice, all integers  $m_p, m_\eta$ , etc., are considered to be equal to a common integer  $m$ . In such case, matrix  $M_{v\eta}$  defined by (A.4) is also square and a similar reasoning allows showing that  $M_{v\eta}$  is invertible (using columns instead of rows).

The proof is here given for matrix  $M_p$  defined by (A.8):

$$[M_p]_{ki} = \int_{\Omega_f} \text{div}(\overline{\text{grad}} \phi_i^p) \phi_k^p d\Omega \quad \forall k \in \{1, \dots, m_p\}, \forall i \in \{1, \dots, m_p\}$$

Let us suppose that  $M_p$  is not invertible. Hence  $M_p$  would not be of rank  $m_p$  meaning that at least one of its rows, let's say row  $\ell$ , would be a linear combination of other rows:

$$\begin{aligned}
[M_p]_{\ell i} &= \sum_{\substack{j=1 \\ j \neq \ell}}^{m_p} \alpha_j [M_p]_{ji} \quad \forall i \in \{1, \dots, m_p\} \\
\Leftrightarrow \int_{\Omega_f} \text{div}(\overline{\text{grad}} \phi_i^p) \phi_\ell^p d\Omega &= \sum_{\substack{j=1 \\ j \neq \ell}}^{m_p} \alpha_j \int_{\Omega_f} \text{div}(\overline{\text{grad}} \phi_j^p) \phi_j^p d\Omega \quad \forall i \in \{1, \dots, m_p\} \\
\Leftrightarrow \int_{\Omega_f} \text{div}(\overline{\text{grad}} \phi_i^p) \left( \phi_\ell^p - \sum_{\substack{j=1 \\ j \neq \ell}}^{m_p} \alpha_j \phi_j^p \right) d\Omega &= 0 \quad \forall i \in \{1, \dots, m_p\} \\
\Leftrightarrow \phi_\ell^p(\bar{x}) &= \sum_{\substack{j=1 \\ j \neq \ell}}^{m_p} \alpha_j \phi_j^p(\bar{x})
\end{aligned}$$

Function  $\phi_p^p(\bar{x})$  would thus be a linear combination of functions  $\phi_j^p(\bar{x}), j \in \{1, \dots, m_p\}, j \neq \ell$ .

This is in contradiction with the definition of functions  $\phi_j^p(\bar{x}), j \in \{1, \dots, m_p\}$  as a truncation of a basis of the Hilbert space formed by the space  $\mathcal{L}_2(\Omega_f)$  of square integrable functions on  $\Omega_f$  equipped with the usual inner product (36).

As a consequence, the assumption “ $M_p$  is not invertible” is not valid and  $M_p$  is invertible.

## A.3 ROMs construction: optimization algorithms

### A.3.1 Particle Swarm Optimization (PSO) for vector $\theta$

A Particle Swarm Optimization (PSO) algorithm [20] has been used for the estimation of vector  $\theta$ . Our home-made PSO code uses a circular neighborhood of size 3. A swarm of  $N_p=20$  particles has been used. At iteration  $k + 1$  of the PSO algorithm, pseudo-velocity  $v_j^{p,k+1}$  and position  $\theta_j^{p,k+1}$  of particle  $p$  in direction  $j$  of the unknown parameters space of dimension  $N_\theta(m)$  are updated according to the following sequence:

$$\begin{aligned} v_j^{p,k+1} &= \chi_{PSO} v_j^{p,k} + \lambda_{PSO} rand_p(\theta_j^{p,best} - \theta_j^{p,k}) + \lambda_{PSO} rand_g(\theta_j^{p,g} - \theta_j^{p,k}) \\ \theta_j^{p,k+1} &= \theta_j^{p,k} + v_j^{p,k+1} \end{aligned}$$

$\theta^{p,best}$  is the best position found by particle  $p$  and  $\theta^{p,g}$  is the best position found by its informants, up to date.  $rand_p$  and  $rand_g$  are random numbers taken from a uniform distribution in  $[0;1]$ . Parameters  $\chi_{PSO} = 0.729$  and  $\lambda_{PSO} = 1.494$  have been used. This set was previously tested in [34]. A parallelized version has been used in the present work: for each particle, equations (56) to (61) corresponding to the vector  $\theta$  associated with the particle, are solved by a dedicated process, for all triplets  $(K, n, Q_{in})_j^{data}, j \in \{1, \dots, N_s^{id}\}$ .

### A.3.2 Ordinary Least Squares for matrix $H$

At each iteration of the PSO algorithm, for each particle of the swarm, parameters in  $\theta$  are fixed: the low order state vector  $\tilde{a}^T(t) \in \mathbb{R}^m$  is computed for all triplets  $(K, n, Q_{in})_j^{data}, j \in \{1, \dots, N_s^{id}\}$  at all instants  $t_k, k \in \{1, \dots, N_t^{id}\}$  by solving equations (56) to (61) as explained in section 4.9.

Matrix  $\mathbb{A} \in \mathbb{R}^{m \times (N_s^{id} N_t^{id})}$  is then formed:

$$\mathbb{A} = \left[ \tilde{a}^T(1, t_1) \cdots \tilde{a}^T(1, t_{N_t^{id}}) \cdots \tilde{a}^T(N_s^{id}, t_1) \cdots \tilde{a}^T(N_s^{id}, t_{N_t^{id}}) \right]$$

Matrix  $\mathbb{T}^{data} \in \mathbb{R}^{N_{obs} \times (N_s^{id} N_t^{id})}$  is formed in a similar way:

$$\begin{aligned} &\mathbb{T}^{data} \\ &= \left[ \delta T_{obs}^{FOM,data}(1, t_1) \cdots \delta T_{obs}^{FOM,data}(1, t_{N_t^{id}}) \cdots \delta T_{obs}^{FOM,data}(N_s^{id}, t_1) \cdots \delta T_{obs}^{FOM,data}(N_s^{id}, t_{N_t^{id}}) \right] \end{aligned}$$

Calling  $\mathbb{T}$  the corresponding matrix for the ROM, one has, according to output equation (62):

$$\mathbb{T} = H\mathbb{A} \quad (\text{A.27})$$

Using the Frobenius norm  $\|M\|_F = (\sum_i \sum_j M_{ij}^2)^{1/2}$  of a real valued matrix  $M$  and equation (A.27), the quadratic functional  $\mathcal{J}_{ident}^{(m)}(\theta, H)$  defined by equation (63) can also be written:

$$\mathcal{J}_{ident}^{(m)}(\theta, H) = \|\mathbb{T} - \mathbb{T}^{data}\|_F^2 = \|\mathbb{T}^t - [\mathbb{T}^{data}]^t\|_F^2 = \|\mathbb{A}^t H^t - [\mathbb{T}^{data}]^t\|_F^2$$

Where “ $t$ ” denotes here the transposition sign.

Using the  $L_2$  norm  $\|V\|_2 = (\sum_i V_i^2)^{1/2}$  of a real valued vector  $V$ ,  $\mathcal{J}_{ident}^{(m)}(\theta, H)$  also writes:

$$\mathcal{J}_{ident}^{(m)}(\theta, H) = \sum_{j=1}^{N_{obs}} \|\mathbb{A}^t (H^t)_j - ([\mathbb{T}^{data}]^t)_j\|_2^2$$

where  $(H^t)_j \in \mathbb{R}^m$  and  $([\mathbb{T}^{data}]^t)_j \in \mathbb{R}^{N_s^{id} N_t^{id}}$  are respectively the  $j^{th}$  column of  $H^t \in \mathbb{R}^{m \times N_{obs}}$  and  $[\mathbb{T}^{data}]^t \in \mathbb{R}^{(N_s^{id} N_t^{id}) \times N_{obs}}$ .

So, for  $\theta$  fixed, searching for  $H$  minimizing  $\mathcal{J}_{ident}^{(m)}(\theta, H)$  is equivalent to minimizing each one of the  $\|\mathbb{A}^t (H^t)_j - ([\mathbb{T}^{data}]^t)_j\|_2^2$ ,  $j \in \{1, \dots, N_{obs}\}$ .  $\mathbb{A}^t \in \mathbb{R}^{(N_s^{id} N_t^{id}) \times m}$  and  $([\mathbb{T}^{data}]^t)_j \in \mathbb{R}^{N_s^{id} N_t^{id}}$  are known, hence under the condition  $N_s^{id} N_t^{id} \geq m$  (easily fulfilled in practice), the estimation of  $(H^t)_j \in \mathbb{R}^m$  using Ordinary Least Squares consists in solving:

$$\mathbb{A} \mathbb{A}^t (H^t)_j = \mathbb{A} ([\mathbb{T}^{data}]^t)_j \quad j \in \{1, \dots, N_{obs}\}$$

Matrix  $H^t$  is therefore estimated by simply solving:

$$\mathbb{A} \mathbb{A}^t H^t = \mathbb{A} [\mathbb{T}^{data}]^t \quad (\text{A.28})$$

## Acknowledgements

The authors wish to thank Professor Rémi Deterre of GEPEA for sharing fruitful discussions.

## References

- [1] S. H. Tabatabaei, P. J. Carreau and A. Ajji, "Effect of processing on the crystalline orientation, morphology, and mechanical properties of polypropylene cast films and microporous membrane formation," *Polymer*, vol. 50, pp. 4228-4240, 2009.
- [2] T. Ageyeva, S. Horváth and J. G. Kovács, "In-Mold Sensors for Injection Molding: On the Way to Industry 4.0," *Sensors*, vol. 19, p. 3551, 2019.
- [3] F. Trochu, E. Ruiz, V. Achim and S. Soukane, "Advanced numerical simulation of liquid composite molding for process analysis and optimization," *Composites Part A: Applied Science and Manufacturing*, vol. 37, pp. 890-902, 2006.

- [4] A. Guevara-Morales and U. Figueroa-López, "Residual stresses in injection molded products," *Journal of Materials Science*, vol. 49, pp. 4399-4415, 2014.
- [5] D. E. Smith, "Design sensitivity analysis and optimization for polymer sheet extrusion and mold filling processes," *International Journal for Numerical Methods in Engineering*, vol. 57, pp. 1381-1411, 2003.
- [6] J. Wang and Q. Mao, "A Novel Process Control Methodology Based on the PVT Behavior of Polymer for Injection Molding," *Advances in Polymer Technology*, vol. 32, p. E474–E485, 2013.
- [7] Z. Chen and L.-S. Turng, "A review of current developments in process and quality control for injection molding," *Advances in Polymer Technology*, vol. 24, pp. 165-182, 2005.
- [8] A. Pabedinskas, W. R. Cluett and S. T. Balke, "Development of an in-line rheometer suitable for reactive extrusion processes," *Polymer Engineering & Science*, vol. 31, pp. 365-375, 1991.
- [9] Q. Lin, N. Allanic, R. Deterre, P. Mousseau and M. Girault, "In-line viscosity identification via thermal-rheological measurements in an annular duct for polymer processing," *International Journal of Heat and Mass Transfer*, vol. 182, p. 121988, 2022.
- [10] Y. Wang, H. Ma, W. Cai, H. Zhang, J. Cheng and X. Zheng, "A POD-Galerkin reduced-order model for two-dimensional Rayleigh-Bénard convection with viscoelastic fluid," *International Communications in Heat and Mass Transfer*, vol. 117, 2020.
- [11] F. Chinesta, A. Ammar, A. Leygue and R. Keunings, "An overview of the proper generalized decomposition with applications in computational rheology," *Journal of Non-Newtonian Fluid Mechanics*, vol. 166, p. 578–592, 2011.
- [12] M. S. Aghighi, A. Ammar, C. Metivier, M. Normandin and F. Chinesta, "Non-incremental transient solution of the Rayleigh-Bénard convection model by using the PGD," *Journal of Non-Newtonian Fluid Mechanics*, vol. 200, pp. 65-78, 2013.
- [13] E. Hernandez-Martinez, J. Vernon-Carter and J. Alvarez-Ramirez, "First-harmonic balance for fast evaluation of power-law fluid flow enhancement under periodic pressure gradient," *Chemical Engineering Science*, vol. 87, pp. 67-74, 2013.
- [14] M. Girault, J. Launay, N. Allanic, P. Mousseau and R. Deterre, "Development of a thermal Reduced Order Model with explicit dependence on viscosity for a generalized Newtonian fluid," *Journal of Non-Newtonian Fluid Mechanics*, vol. 260, pp. 26-39, 2018.

- [15] M. Girault, D. Petit and E. Videcoq, "Identification of Low-Order Models and Their Use for Solving Inverse Boundary Problems," in *Thermal Measurements and Inverse Techniques*, H. R. Orlande, O. Fudym, D. Maillet and R. M. Cotta, Eds., CRC Press, 2011, pp. 457-506.
- [16] M. Girault, E. Videcoq and D. Petit, "Estimation of time-varying heat sources through inversion of a low order model built with the modal identification method from in-situ temperature measurements," *International Journal of Heat and Mass Transfer*, vol. 53, no. 1-3, pp. 206-219, 2010.
- [17] K. Bouderbala, H. Nouria, M. Girault and E. Videcoq, "Experimental thermal regulation of an ultra-high precision metrology system by combining Modal Identification Method and Model Predictive Control," *Applied Thermal Engineering*, vol. 104, pp. 504-515, 2016.
- [18] L. Cordier, M. Girault and D. Petit, "Reduced Order Modeling by Modal Identification Method and POD-Galerkin approach of the heated circular cylinder wake in mixed convection," *Journal of Physics: Conference Series*, vol. 395, no. 1, 2012.
- [19] M. Girault, Y. Liu, Y. Billaud, A. M. Benselama, D. Saury and D. Lemonnier, "Reduced Order Models for conduction and radiation inside semi-transparent media via the Modal Identification Method," *International Journal of Heat and Mass Transfer*, vol. 168, 2021.
- [20] M. Clerc, Particle Swarm Optimization, New-York: Wiley-ISTE, 2013.
- [21] J.-F. Agassant, P. Avenas, P. J. Carreau, B. Vergnes and M. Vincent, Polymer processing: principles and modeling, Carl Hanser Verlag GmbH Co KG, 2017.
- [22] R. B. Bird, "Experimental tests of generalised newtonian models containing a zero-shear viscosity and a characteristic time," *Canadian Journal of Chemical Engineering*, vol. 43, p. 161–168, 1965.
- [23] D. W. McEachern, "Axial laminar flow of a non-Newtonian fluid in an annulus," *AICHE Journal*, vol. 12, p. 328–332, 1966.
- [24] W. Ostwald, "About the rate function of the viscosity of dispersed systems," *Kolloid Zeitschrift*, vol. 36, pp. 99-117, 1925.
- [25] A. de Waele, "Viscometry and plastometry," *Journal of the Oil & Colour Chemists' Association*, vol. 6, pp. 33-88, 1923.
- [26] M. M. Cross, "Rheology of non-Newtonian fluids : A new flow equation for pseudoplastic systems," *Journal of Colloid Science*, vol. 20, no. 5, 1965.

- [27] P. J. Carreau, "Rheological equations from molecular network theories," *Transactions of the Society of Rheology*, vol. 16, pp. 99-127, 1972.
- [28] J. Launay, N. Allanic, P. Mousseau, R. Deterre and C. Plot, "Effect of viscous dissipation in the prediction of thermal behavior of an elastomer cylindrical flow," *Journal of Materials Processing Technology*, vol. 252, pp. 680-687, 2018.
- [29] S. J. Leon, Å. Björck and W. Gander, "Gram-Schmidt orthogonalization: 100 years and more," *Numerical Linear Algebra with Applications*, vol. 20, pp. 492-532, 2013.
- [30] D. K. Gartling and E. B. Becker, "Finite element analysis of viscous, incompressible fluid flow: Part 1 : Basic methodology," *Computer Methods in Applied Mechanics and Engineering*, vol. 8, pp. 51-60, 1976.
- [31] J. Crank and P. Nicolson, "A practical method for numerical evaluation of solutions of partial differential equations of the heat-conduction type," *Mathematical Proceedings of the Cambridge Philosophical Society*, vol. 43, pp. 50-67, 1947.
- [32] B. Beachkofski and R. Grandhi, "Improved distributed hypercube sampling," in *43rd AIAA ASME ASCE AHS ASC Struct. Struct. Dyn. Mater. Conf.*, 2002.
- [33] R. Deterre, P. Mousseau and A. Sarda, *Injection des polymères: simulation, optimisation et conception*, Elsevier, 2003.
- [34] R. C. Eberhart and Y. Shi, "Comparing Inertia Weights and Constriction Factors in Particle Swarm Optimization," in *Proceedings of the IEEE International Congress Evolutionary Computation*, San Diego, 2000.